Precambrian Research 208–211 (2012) 72–89

Contents lists available at SciVerse ScienceDirect

Precambrian Research

journal homepage: www.elsevier.com/locate/precamres

Neoproterozoic eclogites in the Paleoproterozoic Ubendian Belt of Tanzania: Evidence for a Pan-African suture between the Bangweulu Block and the Tanzania Craton

Nelson Boniface[a,*], Volker Schenk[b]

[a] University of Dar es Salaam, P.O. Box 35052, Dar es Salaam, Tanzania
[b] Universität Kiel, Institut für Geowissenschaften, 24098 Kiel, Germany

ARTICLE INFO

Article history:
Received 28 April 2011
Received in revised form 15 March 2012
Accepted 31 March 2012
Available online xxx

Keywords:
Eclogite
Pan-African
Ubendian Belt
Tanzania Craton
Bangweulu Block
Gondwana

ABSTRACT

Geochronological, petrographic and geochemical data from eclogites of the Ufipa Terrane in the Ubendian Belt demonstrate that a Pan-African suture zone dated at 593 ± 20, 548 ± 39 and 524 ± 12 Ma (zircon U–Pb SHRIMP) separates the Tanzania Craton from the Bangweulu Block along the Ubendian Belt. These new and surprising data indicate that during the amalgamation of the Gondwana Supercontinent there was a collision between the Archean Cratons of Tanzania and Bangweulu. A clockwise *P–T* path that climaxed at pressures of 15–20 kbar and temperatures of 610–790 °C were estimated for these eclogites. This indicates a relatively warm subduction with a geothermal gradient of about 10–11 °C/km.

Magmatic precursor rocks of kyanite-free eclogites crystallized in the back-arc (group I eclogite) and island-arc (group II eclogite) tectonic settings. The light rare earth elements (LREEs) of group I eclogites range between 10 and 30 times chondritic values suggesting a depleted mantle source similar to that of mid oceanic ridge basalts (MORB). Group II eclogites display characteristic depletions of high-field-strength elements (Na, Ta, Zr and Hf) relative to LREEs that is typical for island-arc basalts.

The U–Pb zircon ages at 593 ± 20 and 524 ± 12 Ma from the kyanite-free eclogites have a difference of about 70 Ma. The time interval of this much long is not likely to represent a single subduction event. Therefore, it is more likely that successive accretions of volcanic-arc rocks occurred at 593 ± 20, 548 ± 39 and 524 ± 12 Ma.

© 2012 Elsevier B.V. All rights reserved.

1. Introduction

Only few eclogites are known to crop out in the Neoproterozoic orogenic belts of central and southern Africa (Fig. 1). This limits our knowledge about subduction processes and the closure of ocean basins during the formation of the Gondwana supercontinent. Nevertheless, the petrology, geochemistry and geochronology of the few known Pan-African eclogites allows insights into their tectonic setting and timing of subduction. Eclogites of the Zambezi Belt in Zambia have a MORB-like chemistry and experienced their subduction metamorphism at 650–610 Ma (John et al., 2003); the eclogites of northern Malawi, thought to belong to the Mozambique Belt, have the compositions of intraplate basalts and were subducted ca. 530–500 Ma ago (Ring et al., 2002). In addition, the ≈850–700 Ma back-arc/island-arc and continental arc related metabasites of the Vohibory Block in southwestern Madagascar experienced collisional metamorphism at 612 ± 5 Ma (Jöns and Schenk, 2008).

Here we present petrological, geochemical and geochronological data for the eclogites of the Ufipa Terrane in the Ubendian Belt, which allow us deduce the tectonic setting of the basaltic protoliths, determine the timing of eclogite-facies metamorphism, hence subduction, and establish the *P–T* path that was experienced during the subduction process. Our findings provide a new perspective on the spatial and temporal distribution of Pan-African suture zones in Africa. Former simple models of Gondwana formation assumed either that West Gondwana (Congo-Kalahari-Southern America) formed one continental block when Indo-Antarctica and, later, Antarctica-Australia (East Gondwana) amalgamated (Boger and Miller, 2004) or that the Congo-Tanzania-Bangweulu Block formed one continental block throughout the Neoproterozoic (Collins and Pisarevsky, 2005). In this paper we demonstrate that the Bangweulu Block was separated by a Neoproterozoic suture zone from the Tanzania Craton in the north and that it most likely formed a microplate, because the eclogites of the Zambezi Belt were formed from subducted oceanic lithosphere at its southern border (John et al., 2003).

* Corresponding author.
E-mail addresses: nelson.boniface@udsm.ac.tz (N. Boniface), vs@min.uni-kiel.de (V. Schenk).

0301-9268/$ – see front matter © 2012 Elsevier B.V. All rights reserved.
http://dx.doi.org/10.1016/j.precamres.2012.03.014

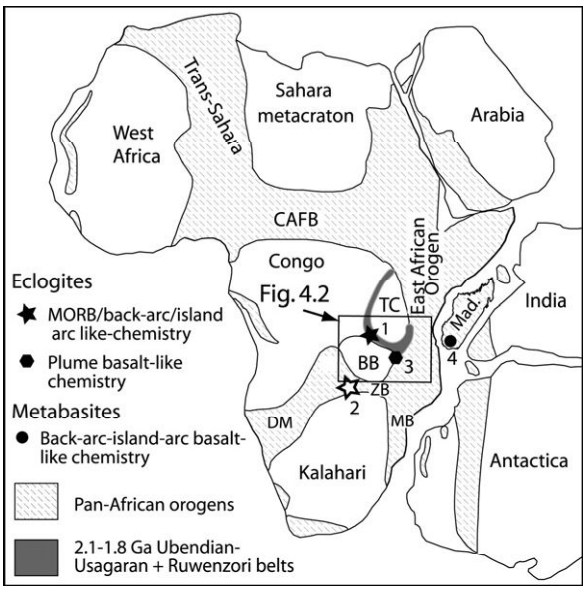


Fig. 1. Pan-African sutures in the central part of Gondwana. (1) Back-arc/island-arc related eclogites in the Paleoproterozoic Ubendian Belt, this study. (2) MORB-like chemistry eclogites in the Pan-African Zambezi Belt (John et al., 2003). (3) Intraplate basalt-like chemistry eclogites in northern Malawi (Ring et al., 2002). (4) Back-arc/island-arc related metabasites in the Vohibory block of Madagascar (Jöns and Schenk, 2008). DM=Damara Belt, ZB=Zambezi Belt, MB=Mozambique Belt, BB=Bangweulu Block, TC=Tanzania Craton, CAFB=Central African Fold Belt, Mad=Madagascar; map modified after Kusky et al. (2003).

2. Analytical techniques

Minerals were analyzed by using a JEOL Superprobe JXA-8900R electron microprobe at the University of Kiel, with an acceleration potential of 15–20 kV for a beam current of 20 nA. The raw data were corrected using the CITZAF method (Armstrong, 1995).

Major element concentrations of whole rocks were analyzed on fused glass discs at the University of Kiel using a Philips PW 1400 X-ray fluorescence analyzer. The disks were prepared by mixing 0.6 g of sample powder with 3.6 g of $Li_2B_4O_7$ in a platinum crucible, which was fused in an OXIFLUX 5-stage burner. Trace element concentrations were determined on an Agilent 75000C ICP-MS at the University of Kiel using the procedure as described by Garbe-Schönberg (1993) and John et al. (2008). The data quality, precision and accuracy were ensured by using international reference standards, measuring blanks and some sample in duplicate. Zircons were separated from crushed rocks using conventional magnetic and heavy liquid methods at the University of Kiel. U–Pb dating of zircon was done on a SHRIMP-II at the Center of Isotopic Research of VSEGEI in St. Petersburg, Russia. Handpicked round and prismatic zircon grains were mounted in epoxy resin discs and polished to expose their cores, then imaged using transmitted light and cathodoluminescence (CL). The diameter of the ion beam was approximately 20 μ and the primary beam intensity was about 4 nA. Data reduction was done following Williams (1998), using the SQUID Excel Makro by Ludwig (2001). The Pb/U ratios were normalized relative to a value of 0.0668 for the $^{206}Pb/^{238}U$ ratio of the TEMORA-1 internal standard reference zircon, equivalent to an age of 416.75 Ma (Black et al., 2003).

3. Geological background

The NW-SE elongated Ubendian Belt (ca. 500 km long and 150 km wide) is bordered by the Archean Cratons of Tanzania to the northeast and Bangweulu to the southwest. The Ubendian Belt is bordered to the northwest by the N-S trending Mesoproterozoic Kibaran Belt and to the SE by the Paleoproterozoic Usagaran Belt and the N-S oriented Neoproterozoic East African Orogen (Fig. 2).

On the basis of structural and lithological differences, Daly et al. (1985) and Daly (1988) divided the Ubendian Belt into eight terranes, namely the Ubende, Wakole, Katuma, Ufipa, Mbozi, Lupa, Upagwa, and Nyika lithotectonic terranes (Fig. 2). Further structural studies on different terranes of the Ubendian Belt done by Theunissen et al. (1996), Boven et al. (1999) revealed complex and different structural element orientation in different terranes. For instance analyses of the moderate to steeply dipping schistosity and gneissic fabric display regional W-E orientated π-axis in the Ubende Terrane and NW-SE orientated π-axis in the Ufipa Terrane. Terrane boundaries (marked in Fig. 2) constitute tracts of mylonites to ultra-mylonites, and gouge displaying dextral sense of shear with π-axis orientation sub-parallel to NW-SE (Daly, 1988; Theunissen et al., 1996; Boven et al., 1999). The boundary between the Ubendian Belt (along the Ufipa Terrane) and the Archean Bangweulu Block (Craton) is characterized by the presence of a shear zone and a transition from the high-grade sillimanite–cordierite migmatitic gneisses in the Ufipa Terrane to the low-grade muscovite–biotite schists with W-E fabric in the Bangweulu Block (e.g. De Waele et al., 2006, and references therein).

Our own unpublished data and the work of Boniface et al. (2012) further indicate a largely heterogeneous nature of the Ubendian Belt to be reflected in the distribution of ages of the Neoproterozoic and the Mesoproterozoic metamorphic cycles among the terranes. The Mesoproterozoic metamorphic ages in metapelites are solely confined in the northwestern terranes of Ubende and Wakole no such ages were detected in the terranes of Ufipa and Mbozi. In the contrary, the Neoproterozoic metamorphic ages in metapelites and other lithological units were detected in all the terranes except the Wakole.

Eclogites in the Ubendian Belt crop out in the terranes of Ufipa and Ubende. Boniface and Schenk (2007) and Boniface et al. (2012) have demonstrated that the eclogites of the Ubende Terrane were formed during a Paleoproterozoic orogenic cycle (1890–1860 Ma) and those of the Ufipa Terrane belong to the Neoproterozoic suture zone. The Ubende Terrane Paleoproterozoic eclogites crop out as mylonitic pods within felsic garnet–clinopyroxene gneisses and hornblende-rich mafic gneisses, whereas the Neoproterozoic eclogites described in this contribution are exposed in the Ufipa Terrane as massive lense-shaped bodies (10–100 m scale) enclosed in garnet–kyanite mica schists and gneisses. The eclogites of the Ufipa Terrane are coarse-grained and were not deformed following peak metamorphism, in contrast to the Paleoproterozoic eclogites of the Ubende Terrane, which are fine-grained and mylonitized. The occurrence of eclogites in the Ubendian Belt has been known since the reports of Smirnov et al. (1973). Sklyarov et al. (1998) determined the *P–T* evolution for the eclogites of the Ubendian Belt. However, in the absence of geochronological data, these authors mixed together petrological data from the Paleoproterozoic and Neoproterozoic eclogites to deduce a single *P–T* evolution for these Ubendian rocks of different ages. It was assumed that eclogites of the Ubendian Belt are synchronous with the 2.0 Ga eclogites, dated by Möller et al. (1995), from the Usagaran Belt (Fig. 2).

The Ufipa Terrane, which hosts the Neoproterozoic eclogites, is dominated by biotite-gneiss of granitic composition (McConnell, 1950; Sutton et al., 1954). However, other lithological units like metapelites are present: garnet–biotite–kyanite–muscovite gneisses and schists are interlayered with eclogites and crop out in northern Ufipa Terrane near Chisi and Tambaruka villages, whereas garnet–biotite–sillimanite ± cordierite gneisses and schists are found in southern part of the Ufipa Terrane (Fig. 3). The transition from muscovite–quartz to higher-grade sillimanite (kyanite)-K-feldspar gneisses is near the town of Sumbawanga. Our own unpublished U–Th total Pb monazite data suggest that

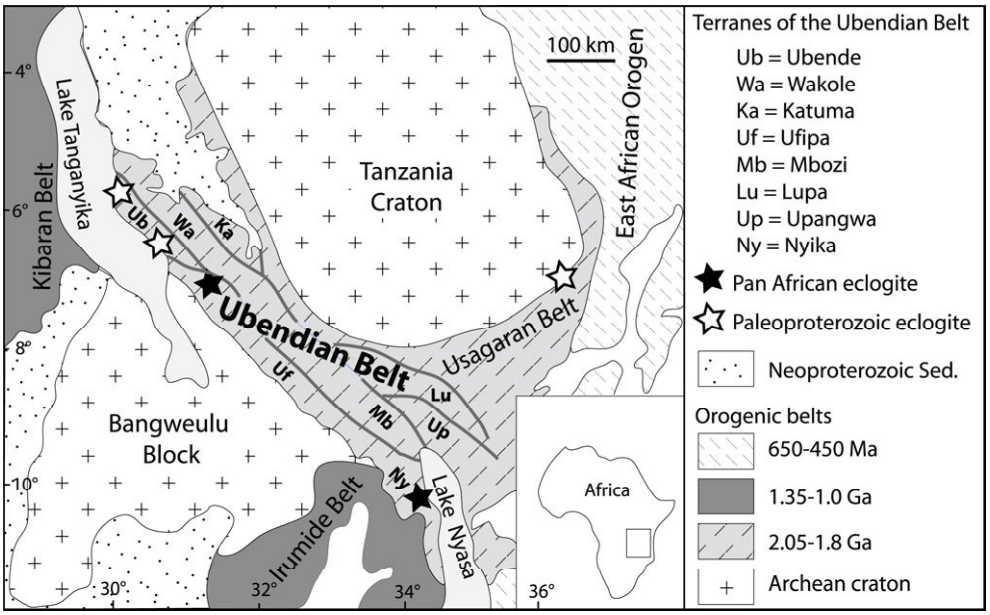


Fig. 2. Geological map of south-eastern Africa indicating the location of the Ubendian Belt. Subdivision in litho-tectonic terranes by Daly et al. (1985) and Daly (1988).

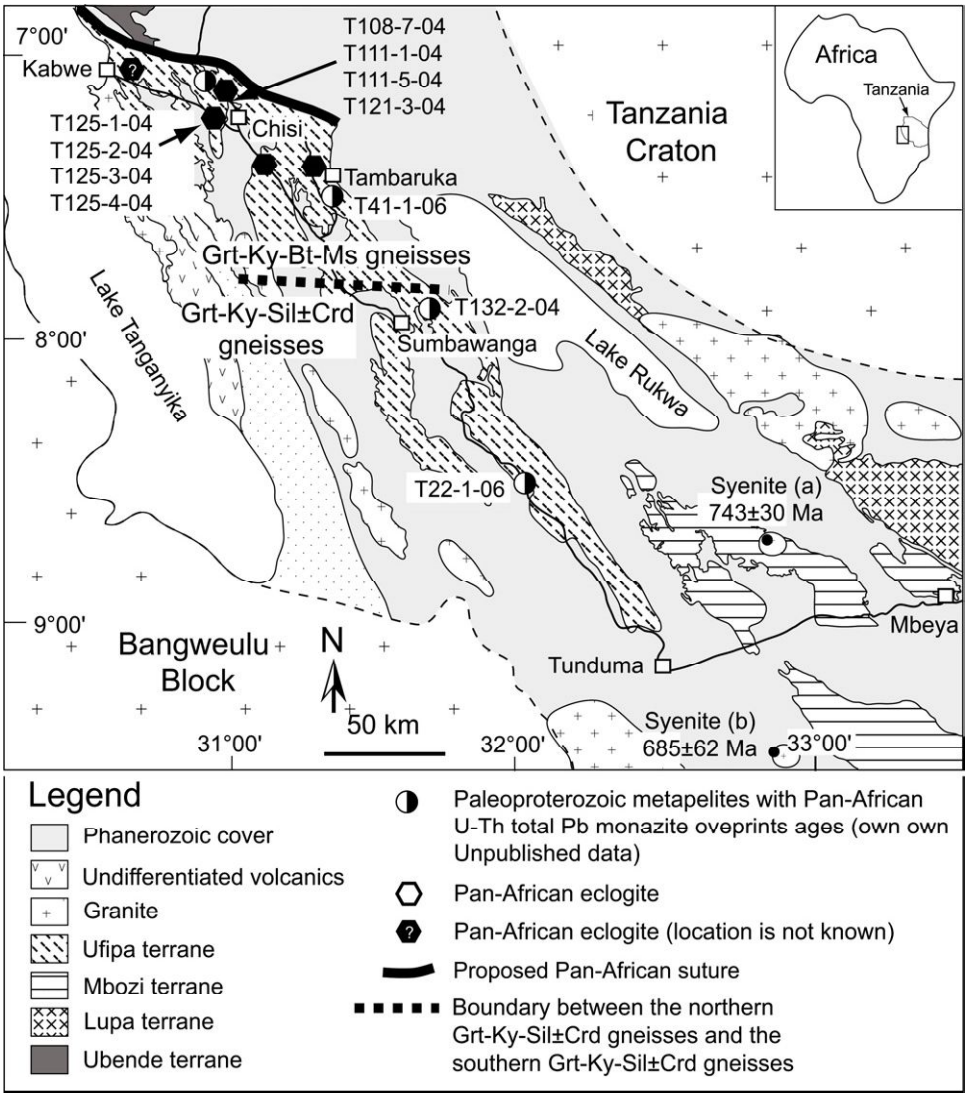


Fig. 3. Locations of Pan-African eclogites in the Ubendian Belt. Ages of Pan-African syenites in the Mbozi Terrane are from (a) Brock (1963) and (b) Ray (1974). The zircon and/or monazite of four metapelites of the Ufipa Terrane show a strong Neoproterozoic overprint.

metapelites of the Ufipa Terrane were strongly reworked in the Neoproterozoic Eon, which we link with the Pan-African subduction zone metamorphism described in this contribution.

Alkali and syenite intrusions, which pre-date the Pan-African orogenic cycle occur in the Ubendian Belt. Alkali-granitoids were dated at 724 ± 6 Ma by Theunissen et al. (1992) and at 842 ± 80 Ma by Lenoir et al. (1994) in the Upangwa Terrane (U–Pb zircon dissolution); syenites in the Mbozi Terrane were dated at 743 ± 30 (Brock, 1963) and 685 ± 62 Ma (Ray, 1974) (Rb–Sr) (Fig. 3). These early pre Pan-African magmatic events may reflect a time of extension preceding the subduction and collision in the Ubendian Belt.

4. Petrography and geochemistry

On the basis of mineralogy, the Neoproterozoic eclogites of the Ufipa Terrane fall into two groups: kyanite-free and kyanite-bearing eclogites; each are discussed in turn.

4.1. Kyanite-free eclogites

The kyanite-free eclogites are composed of omphacite (clinopyroxene)–garnet–rutile–apatite–quartz–zircon as the peak mineral assemblage, where omphacite and garnet occupy up to 90% by volume. Rutile, reaching up to 0.5 mm in diameter, is a common matrix mineral and occurs also as inclusions in garnet and clinopyroxene. Garnet contains prograde inclusions of plagioclase, rutile, quartz and omphacite (Fig. 4A). Abundant plagioclase–diopside symplectites replace omphacite, whereas hornblende coronas sometimes occur between garnet and omphacite (Fig. 4B). The abundance of retrograde minerals, diopside–plagioclase and hornblende, differs from sample to sample, in which the least retrogressed rocks may contain less than 5% by volume of the late-stage minerals.

The compositions of garnet, omphacite, plagioclase and hornblende are given in Tables 1–3; see Footnote [1] Garnet cores are homogeneous and pyrope-rich (X_{Prp}=0.48, X_{Alm}=0.39, X_{Grs}=0.12 and X_{Sps}=0.01) and are surrounded by retrograde rims, 0.1–0.3 mm wide, in which X_{Prp} (0.41) drops and X_{Alm} (0.44) rises (Fig. 5A). In one sample (T121-3-04), garnet is almandine rich with a composition of X_{Alm}=0.47, X_{Prp}=0.33, X_{Grs}=0.19 and X_{Sps}=0.01 (Table 1; see Footnote 1). Cores of clinopyroxene porphyroblasts and inclusions in garnet are rich in Na, with jadeite contents up to 40 mol%. By contrast, clinopyroxene in the symplectites is poor in Na, with molar jadeite between 20 and 11 mol% (Fig. 5C and Table 2; see Footnote 1. The X_{Mg} (X_{Mg}= Mg/(Fe + Mg)) is high in all clinopyroxenes, ranging between 0.70 and 0.87 (Table 2; see Footnote 1). Plagioclase in symplectites is richer in Na (X_{Ab} = 0.75 – –0.80) than the plagioclase inclusions in garnet (X_{Ab} = 0.63 – 0.68; Table 3; see Footnote 1). Rutile coexisting with zircon and quartz has average Zr contents between 207 ± 8 ppm and 316 ± 24 ppm (Table 7).

4.2. Kyanite-bearing eclogites

The kyanite-bearing eclogites are composed of a peak mineral assemblage of kyanite–garnet–omphacite (clinopyroxene)–rutile–zoisite–quartz–plagioclase–zircon. Kyanite is blue and coarse-grained, up to ≈ 2 cm in length. It contains inclusions of rutile, ±quartz, omphacite, garnet, plagioclase, ±zoisite and, in one sample, staurolite (Fig. 4C and D). Garnet coronas, up to ≈3 mm wide, commonly enclose kyanite (Fig. 4C and D). However, garnet porphyroblasts with inclusions of omphacite, rutile, plagioclase and quartz are abundant in the matrix. Plagioclase in the matrix is regarded as a peak mineral, however, secondary plagioclase replacing omphacite, garnet and kyanite is also abundant. Abundant symplectites of plagioclase, hornblende and ilmenite commonly replace omphacite and garnet (Fig. 4E), whereas silica poor domains, characterized by symplectites of staurolite, spinel, plagioclase and corundum commonly occur between kyanite and garnet (Fig. 4F). Clinopyroxene is partly replaced by plagioclase–diopside ± hornblende in the form of symplectites or sieve textures (Fig. 4B). Sanders et al. (1987) regarded the sieve textures to be equivalent to symplectites. They are interpreted to be formed during decompression under high temperatures and/or during long periods of retrogression.

The compositions of garnet, clinopyroxene, plagioclase, spinel, staurolite and zoisite are given in Tables 4–6; see Footnote 1. Garnet is Fe- and Ca-rich, with homogeneous core compositions of X_{Alm} = 0.44, X_{Grs} = 0.33, X_{Prp} = 0.21 and X_{Sps} = 0.02 (Fig. 5B). The X_{Prp} and the X_{Mg} show a slight increase and an abrupt drop near the margins whereas X_{Grs} decreases towards the rims (Fig. 5B). The garnet corona around kyanite has X_{Grs} of about 0.24, which is lower than that of cores of garnet porphyroblasts. Other contents are similar to the rims of garnet porphyroblasts (Table 6; see Footnote 1).

Clinopyroxene porphyroblasts are zoned: jadeite content drops from about 37 mol% in the core to about 7 mol% at the rims. Clinopyroxene inclusions in garnet are Na-rich, with jadeite contents up to 44 mol% (Fig. 5D, Table 4; see Footnote 1). Their X_{Mg} range between 0.64 and 0.71 (Table 4; see Footnote 1). Matrix plagioclase is zoned, its core has X_{Ab} = 0.87 which drops to 0.77 on the rims (Fig. 5E). Plagioclase inclusions in garnet are also Na-rich, with X_{Ab} between 0.78 and 0.83. Plagioclase in the plagioclase–diopside symplectites replacing omphacite and in the plagioclase–hornblende–ilmenite–symplectites between garnet and omphacite have lower contents of Na, with X_{Ab} ranging between 0.24 and 0.46 (Table 5; see Footnote 1). Staurolite in symplectites has little ZnO, which ranges between 0.02 and 0.04 wt%; it has more Mg than most amphibolite–facies staurolites (X_{Mg} = 0.31; Table 6; see Footnote 1). Spinel in symplectites between garnet coronas and kyanite have X_{Mg} ratios that range between 0.36 and 0.39 (Table 6; see Footnote 1).

5. Mineral reaction history

5.1. Kyanite-free eclogites

Kyanite-free eclogites preserve mainly retrograde reactions. The prograde history is reflected by the inclusions of omphacite, plagioclase and quartz in garnet porphyroblasts. Hornblende coronas formed by replacement of omphacite and garnet (Fig. 4B). The addition of fluids (H_2O) to the dry garnet–omphacite assemblage during uplift was necessary for the formation of these coronas. Plagioclase–diopside symplectites formed by replacing omphacite at lower pressure conditions.

5.2. Kyanite-bearing eclogites

Garnet coronas around kyanite and staurolite inclusions in kyanite (Fig. 4C and D) appear to represent the relics of prograde reactions during subduction. The garnet–kyanite assemblage may partly have formed at the expense of staurolite and quartz that is included in kyanite. The garnet corona may also form as a reaction product between omphacite and kyanite, as described for similar textures in ultra high-pressure granulites and eclogites of Poland (Klemd and Bröcker, 1999).

During uplift coronas of garnet around kyanite reacted with the enclosed kyanite in the presence of water to form corundum-spinel–plagioclase–staurolite symplectites (Fig. 4F).

[1] Excel spreadsheets with data for mineral composition (Tables 1–6), whole-rock geochemistry (Table 8), and geochronology (Table 9) can be accessed in supplementary materials available online.

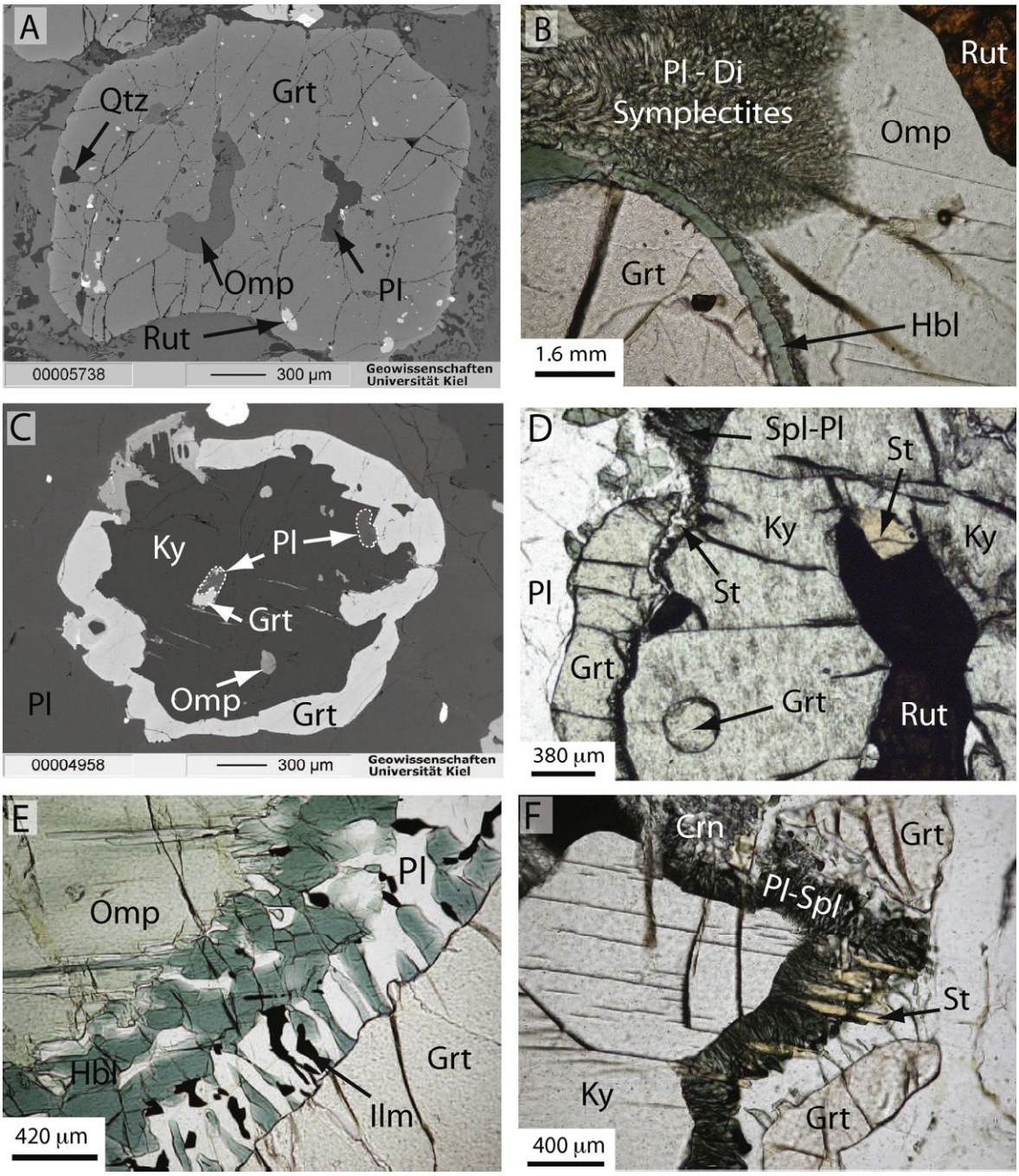


Fig. 4. Microphotographs showing reaction textures in eclogites; backscattered images (A and C) and plane polarized light images (B, D, E and F). (A) Omp, Pl and Rt inclusions in Grt (T111-1-04). (B) Pl–Di symplectites and Hbl corona replacing Omp (T111-5-04). (C) Grt corona around Ky; Omp, Pl and Grt inclusions in Ky (T125-4B-04). (D) St and Grt inclusion in Ky; Grt corona around Ky (T125-3-4). (E) Pl–Hbl–Ilm symplectites between Grt and Omp (T125-1-04). (F) Spl-St-Pl-Crn symplectites between Ky and Grt corona (T125-1-04).

Simultaneously during uplift garnet and omphacite reacted to form the symplectites of hornblende, plagioclase and ilmenite (Fig. 4E). Water addition was necessary to produce hornblende ($Grt + Omp + H_2O = Hbl + Pl + Ilm$; abbreviations for minerals is according to Whitney and Evans (2010)).

6. Geothermobarometry

A summary of the estimates of the prograde (subduction), peak and retrograde (uplift) pressure and temperature conditions that are recorded in the eclogites is given in Table 7. The mineral assemblages and textures of the kyanite-bearing eclogites make it possible to calculate a *P–T* path and to estimate the *P–T* conditions at different stages during subduction and uplift. The peak mineral assemblage Grt–Pl–Ky–Zo–Qz–Rt yields a peak pressure of 20.1 ± 3.4 kbar and a temperature of 785 ± 81 °C as calculated by the average *P–T* method with the THERMOCALC program of Holland and Powell (1998). Mineral core compositions were used for the calculations. Activities of components were calculated by using the AX-program of Holland (version 0.1, 2004). A pressure of ca. 20 kbar is obtained from the GASP equilibrium (Koziol, 1989), calculated by using homogeneous cores of garnet and plagioclase at the inferred temperature of 785 °C using THERMOCALC (Fig. 6A and Table 7).

Table 1
Representative electron microprobe analyses of garnet of the kyanite-free eclogites.

	T108-7 90 core	T108-7 91 core	T108-7 92 core	T108-7 93 core	T111-5 28 rim	T111-5 40 core	T111-5 41 core	T111-5 202 core	T111-5 48 rim	T121-3 56 core	T121-3 59 core	T121-3 60 core	T121-3 73 rim
SiO_2	40.18	40.19	39.72	40.31	39.77	39.99	40.28	40.10	39.72	39.66	39.61	39.81	39.71
Al_2O_3	22.96	22.76	22.44	22.64	22.11	22.50	22.57	22.45	22.13	21.97	21.93	21.88	22.07
FeO	18.91	19.12	18.99	19.01	21.43	19.14	19.16	18.73	22.35	21.93	22.22	22.09	23.15
MgO	12.25	12.09	12.07	12.12	11.30	13.24	13.33	13.22	10.83	9.18	8.81	9.01	8.64
MnO	0.50	0.40	0.38	0.38	0.66	0.39	0.58	0.50	0.65	0.42	0.35	0.48	0.40
CaO	5.84	5.91	5.97	5.89	4.74	4.73	4.87	4.98	4.71	7.24	7.20	7.23	6.63
Total	100.64	100.49	99.59	100.37	100.01	99.99	100.79	99.98	100.39	100.46	100.18	100.60	100.67
Si	2.98	2.99	2.98	3.00	3.00	2.98	2.98	2.99	3.00	3.01	3.01	3.01	3.01
Al	2.01	2.00	1.99	1.99	1.97	1.98	1.97	1.97	1.97	1.96	1.97	1.95	1.97
Fe	1.17	1.19	1.19	1.18	1.35	1.19	1.19	1.17	1.41	1.39	1.41	1.40	1.47
Mg	1.36	1.34	1.35	1.34	1.27	1.47	1.47	1.47	1.22	1.04	1.00	1.02	0.98
Mn	0.03	0.03	0.02	0.02	0.04	0.02	0.04	0.03	0.04	0.03	0.02	0.03	0.03
Ca	0.46	0.47	0.48	0.47	0.38	0.38	0.39	0.40	0.38	0.59	0.59	0.59	0.54
Total	8.01	8.01	8.02	8.01	8.01	8.02	8.03	8.02	8.02	8.01	8.00	8.00	8.00
X_{Mg}	0.54	0.53	0.53	0.53	0.48	0.55	0.55	0.44	0.46	0.43	0.41	0.42	0.40
X_{Alm}	0.39	0.39	0.39	0.39	0.44	0.39	0.39	0.38	0.46	0.46	0.47	0.46	0.49
X_{Prp}	0.45	0.44	0.44	0.44	0.42	0.48	0.48	0.48	0.40	0.34	0.33	0.34	0.32
X_{Grs}	0.15	0.16	0.16	0.16	0.13	0.12	0.12	0.13	0.13	0.19	0.19	0.19	0.18
X_{Sps}	0.01	0.01	0.01	0.01	0.01	0.01	0.01	0.01	0.01	0.01	0.01	0.01	0.01

Cations calculated on the basis of 12 oxygen.

The prograde *P–T* conditions of the Grt–Omp–Pl–Qz mineral assemblage enclosed in kyanite porphyroblasts were constrained by using different geothermobarometers. The THERMOCALC program gives an average pressure of 15.5 ± 3.0 kbar and a temperature of 715 ± 108 °C. The GASP (Koziol, 1989) and the Ab=Jd+Qz (Holland, 1980) geobarometers give similar pressures of 16 kbar at the inferred temperature of 715 °C, which is consistent with the calculated average *P–T* above.

Different geothermobarometers give similar *P–T* conditions for the retrograde formation of the Spl–St–Pl–Crn symplectites between garnet corona and kyanite and the hornblende–plagioclase symplectites between garnet and clinopyroxene (Fig. 4E and F). The THERMOCALC program yields an average pressure of 11.0 ± 3.5 kbar and a temperature of 700 ± 131 °C for the spinel-staurolite-plagioclase-corundum symplectites coupled with kyanite and garnet corona composition. The Grt + Ky = An + Crn equilibrium, which is equivalent to GASP in the absence of Qz (Indares and Rivers, 1995), results in a pressure estimate of 12 kbar at a reference temperature of 700 °C, when using garnet corona composition and plagioclase symplectites. The Grt–Hbl Fe–Mg

Table 2
Representative electron microprobe analyses of clinopyroxene of the kyanite-free eclogites. Calculations of Jd%, F^{3+}, and other cations see Morimoto et al. (1988).

Sample No.	T108-7 91 core	T108-7 79 core	T108-7 93 core	T108-7 94 core	T111-5 176 incl.	T111-5 177 incl.	T111-5 200 core	T111-5 203 core	T111-5 72 symp.	T111-5 77 symp.	T121-3 15 core	T121-4 42 core	T121-5 44 core
SiO_2	54.89	54.03	54.79	54.96	54.23	54.57	55.44	54.55	52.23	52.43	53.15	53.72	53.84
TiO_2	0.15	0.13	0.30	0.26	0.00	0.00	0.00	0.00	0.49	0.38	0.34	0.28	0.34
Al_2O_3	10.01	9.61	10.13	10.12	9.92	10.50	9.85	9.91	6.71	3.84	7.17	6.87	6.83
Cr_2O_3	0.07	0.06	0.05	0.13	0.05	0.07	0.01	0.09	0.00	0.11	0.08	0.06	0.04
FeO	3.49	2.51	4.15	4.3	5.28	5.28	6.39	5.57	5.43	5.06	4.46	5.37	5.36
Fe_2O_3	2.39	3.94	1.85	1.87	2.45	1.94	0.97	1.98	2.52	1.86	3.09	2.4	2.06
MgO	9.17	9.33	9.24	9.22	8.45	8.69	8.44	8.48	11.23	13.22	10.70	10.63	10.76
MnO	0.07	0.10	0.05	0.03	0.01	0.09	0.06	0.08	0.07	0.09	0.04	0.01	0.08
CaO	14.04	15.12	13.82	14.00	13.41	14.05	13.39	13.60	19.00	20.70	16.89	16.97	17.01
Na_2O	5.99	5.63	5.91	5.87	5.89	5.69	5.96	5.83	2.81	1.68	4.02	3.97	3.94
K_2O	0.03	0.00	0.00	0.01	0.00	0.00	0.00	0.00	0.00	0.00	0.00	0.00	0.00
Total	100.30	100.45	100.29	100.77	99.69	100.88	100.51	100.09	100.49	99.37	99.94	100.28	100.26
Si	1.96	1.94	1.96	1.96	1.96	1.96	1.99	1.97	1.91	1.94	1.94	1.95	1.95
Ti	0.00	0.00	0.01	0.01	0.00	0.00	0.00	0.00	0.01	0.01	0.01	0.01	0.02
Al	0.43	0.41	0.43	0.42	0.42	0.44	0.42	0.42	0.29	0.17	0.31	0.29	0.29
Cr	0.00	0.00	0.00	0.00	0.00	0.00	0.00	0.00	0.00	0.00	0.00	0.00	0.00
Fe^{2+}	0.10	0.08	0.12	0.13	0.16	0.16	0.19	0.17	0.17	0.16	0.14	0.16	0.16
Fe^{3+}	0.06	0.11	0.05	0.05	0.07	0.05	0.03	0.05	0.07	0.05	0.08	0.07	0.06
Mg	0.49	0.50	0.49	0.49	0.46	0.46	0.45	0.46	0.61	0.73	0.58	0.58	0.58
Mn	0.00	0.00	0.00	0.00	0.00	0.00	0.00	0.00	0.00	0.00	0.00	0.00	0.00
Ca	0.54	0.58	0.53	0.53	0.52	0.54	0.51	0.52	0.74	0.82	0.66	0.66	0.66
Na	0.42	0.39	0.41	0.41	0.41	0.39	0.41	0.41	0.20	0.12	0.28	0.28	0.28
K	0.00	0.00	0.00	0.00	0.00	0.00	0.00	0.00	0.00	0.00	0.00	0.00	0.00
Total	4.00	4.01	4.00	4.00	4.00	4.00	4.00	4.00	4.00	4.00	4.00	4.00	4.00
X_{Mg}	0.83	0.86	0.80	0.79	0.74	0.74	0.70	0.73	0.78	0.82	0.81	0.78	0.78
Jd (%)	38	34	38	38	38	39	40	38	18	11	24	25	26
Ac (%)	3.5	4.9	2.5	2.4	2.9	0.3	1.2	2.1	2.1	1.5	4.0	3.4	2.3

Cations calculated on the basis of 6 oxygen; incl. = Cpx inclusion in Grt, symp. = symplectites.

Table 3
Representative electron microprobe analyses of plagioclase and hornblende of the kyanite-free eclogites.

Sample T111-5												
Hornblende corona					Plagioclase inclusion in garnet					Symplectite		
No.	6	7	8	13		140	157	158	159	50	53	55
SiO_2	42.30	41.66	41.91	42.03	SiO_2	58.69	60.05	58.69	59.03	63.34	63.99	63.66
TiO_2	0.27	0.26	0.21	0.24	Al_2O_3	26.46	26.08	26.10	25.98	22.70	22.11	20.73
Al_2O_3	15.27	16.67	16.23	15.65	Fe_2O_3	0.39	0.32	0.28	0.22	0.30	0.26	0.72
Cr_2O_3	0.05	0.04	0.06	0.02	CaO	7.52	6.28	6.70	6.45	4.10	3.62	5.36
FeO	10.32	10.51	10.76	11.01	Na_2O	7.05	7.50	7.20	7.35	8.90	9.17	8.84
MgO	13.85	13.45	13.63	13.46	K_2O	0.03	0.05	0.04	0.04	0.03	0.00	0.00
MnO	0.07	0.11	0.13	0.10	Total	100.15	100.28	99.01	99.07	99.42	99.15	99.34
CaO	10.37	9.90	9.62	10.11								
Na_2O	3.48	3.74	3.85	3.44								
Total	95.98	96.33	96.39	96.07								
Si	6.24	6.13	6.16	6.21	Si	2.62	2.66	2.64	2.65	2.81	2.84	2.84
Ti	0.03	0.03	0.02	0.03	Al	1.39	1.36	1.38	1.37	1.19	1.16	1.09
Al	2.66	2.89	2.81	2.73	Fe^{3+}	0.01	0.01	0.01	0.01	0.01	0.01	0.02
Cr	0.01	0.00	0.01	0.00	Ca	0.36	0.30	0.32	0.31	0.20	0.17	0.26
Fe	1.27	1.29	1.32	1.36	Na	0.61	0.64	0.63	0.64	0.77	0.79	0.77
Mg	3.05	2.95	2.99	2.97	K	0.00	0.00	0.00	0.00	0.00	0.00	0.00
Mn	0.01	0.01	0.02	0.01	Total	4.99	4.98	4.98	4.98	4.97	4.97	4.98
Ca	1.64	1.56	1.52	1.60								
Na	1.00	1.07	1.10	0.99								
Total	15.91	15.93	15.95	15.90								
X_{Mg}	0.71	0.70	0.69	0.69	X_{Ab}	0.63	0.68	0.66	0.67	0.79	0.82	0.75
					X_{An}	0.37	0.32	0.34	0.33	0.21	0.18	0.25
					X_{Or}	0.00	0.00	0.00	0.00	0.00	0.00	0.00

Cations calculated on the basis of 8 oxygen for plagioclase and 23 for hornblende.

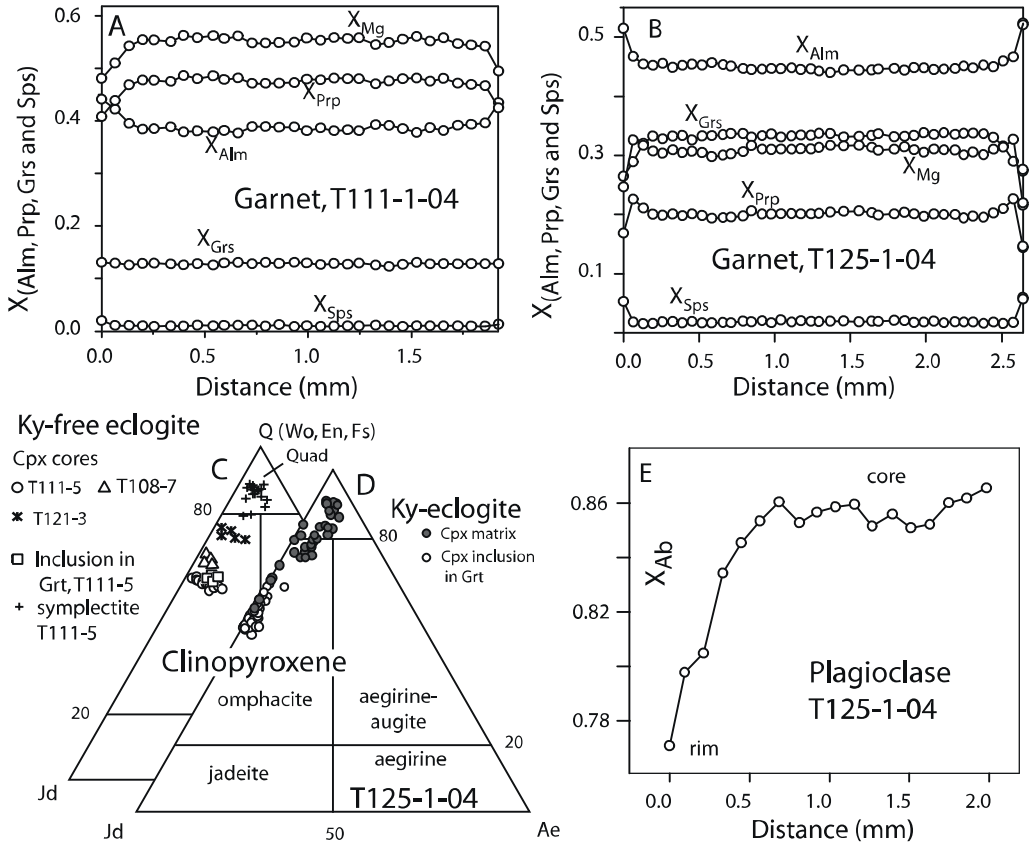


Fig. 5. (A) Garnet profile of a kyanite-free eclogite. (B) Grt profile of a kyanite-bearing eclogite. (C) Cpx composition in kyanite-free eclogites; classification after Morimoto et al. (1988). (D) Cpx composition of the kyanite-bearing eclogites. (E) Pl profile of the kyanite-bearing eclogite.

Table 4
Representative electron microprobe analyses of garnet and clinopyroxene of the kyanite-bearing eclogites. For the calculations of Jd%, F^{3+}, and other cations in pyroxenes see Morimoto et al. (1988).

	T125-2 289 core Garnet	T125-2 290 core	T125-1 523 core	T125-2 265 rim	T125-1 298 corona	T125-4 98 inc.	T125-4 119 inc.		T125-4 80 inc. Clinopyroxene	T125-4 126 inc.	T125-1 160 inc.
SiO_2	38.92	38.86	38.72	38.54	39.12	39.29	39.43	SiO_2	51.81	52.23	53.77
TiO_2	0.11	0.12	0.00	0.05	0.00	0.10	0.06	TiO_2	0.15	0.44	0.35
Al_2O_3	22.02	21.89	21.67	21.39	21.97	21.90	21.83	Al_2O_3	11.09	12.96	14.13
FeO	19.94	19.51	20.69	23.12	22.71	21.99	22.30	Cr_2O_3	0.02	0.00	0.00
MgO	5.59	5.50	4.86	4.10	6.91	6.77	6.47	FeO	5.66	6.74	5.84
MnO	0.65	0.73	0.81	2.18	0.62	0.49	0.54	Fe_2O_3	2.05	0.00	0.00
CaO	12.80	13.15	13.31	10.64	8.93	9.21	9.39	MgO	7.91	6.81	6.40
Total	100.03	99.75	100.06	100.02	100.26	99.75	100.02	MnO	0.04	5.79	0.02
								CaO	16.57	14.27	13.43
								Na_2O	4.53	0.08	6.27
								K_2O	0.01	0.02	0.03
								Total	99.84	99.34	100.24
Si	2.99	2.99	2.99	3.01	3.00	3.02	3.02	Si	1.89	1.91	1.92
Ti	0.01	0.01	0.00	0.00	0.00	0.01	0.00	Ti	0.00	0.01	0.01
Al	1.99	1.99	1.98	1.97	1.99	1.98	1.97	Al	0.48	0.56	0.59
Fe	1.28	1.26	1.34	1.51	1.46	1.41	1.43	Cr	0.00	0.00	0.00
Mg	0.64	0.63	0.56	0.48	0.79	0.78	0.74	Fe^{2+}	0.17	0.21	0.17
Mn	0.04	0.05	0.05	0.14	0.04	0.03	0.04	Fe^{3+}	0.06	0.00	0.00
Ca	1.05	1.09	1.10	0.89	0.73	0.76	0.77	Mg	0.43	0.37	0.34
Total	8.00	8.02	8.02	8.00	8.01	7.99	7.97	Mn	0.00	0.18	0.00
								Ca	0.65	0.56	0.51
								Na	0.32	0.01	0.43
								K	0.00	0.00	0.00
								Total	4.00	3.81	3.97
X_{Mg}	0.33	0.34	0.30	0.24	0.35	0.35	0.34	X_{Mg}	0.72	0.64	0.67
X_{Alm}	0.43	0.42	0.44	0.50	0.48	0.47	0.48	Jd (%)	32	41	44
X_{Prp}	0.21	0.21	0.18	0.16	0.26	0.26	0.25	Ac (%)	0.00	0.00	0.00
X_{Grs}	0.35	0.35	0.36	0.30	0.24	0.26	0.26				
X_{Sps}	0.01	0.02	0.02	0.05	0.02	0.01	0.01				

Cations calculated on the basis of 12 oxygen for Grt and 6 for Cpx; inc. = inclusions in Grt or Ky.

exchange thermometry (Graham and Powell, 1984) combined with Grt–Pl–Hbl geobarometry (Kohn and Spear, 1990) yield a temperature of 740 °C and a pressure of ca. 10 kbar, when using the composition of symplectitic Hbl and Pl coupled with Grt rims. These data lead to the conclusion that the symplectites formed when the pressure dropped nearly isothermally from peak eclogite-facies conditions at about 20 kbar (T = 760–790 °C) to amphibolite–facies conditions of about 10–12 kbar and 700–740 °C (Fig. 6A).

Like the kyanite-bearing eclogite, also garnet porphyroblasts of kyanite-free eclogites contain inclusions of the prograde assemblage Pl–Omp–Qz that allow the estimation of pressure and

Table 5
Representative electron microprobe analyses of plagioclase of the kyanite-bearing eclogites.

Sample	T125-1 Plagioclase	T125-3	T125-1	T125-2	T125-2	T125-2	T125-2	T125-2	T125-2	T125-1	T125-1	T125-2
No.	273 rim	274 rim	290 core	31 core	26 sym. 2	260 sym. 1	264 sym. 1	19 sym. 2	26 sym. 2	395 sym. 1	443 inc.	109 inc.
SiO_2	62.33	63.07	65.31	64.44	64.23	52.32	50.53	50.02	54.76	59.59	63.08	63.97
Al_2O_3	23.07	22.87	21.53	21.53	21.46	30.70	31.16	32.15	28.89	25.54	23.18	22.35
Fe_2O_3	0.05	0.00	0.14	0.12	0.12	0.67	0.84	0.45	0.32	0.24	0.12	0.29
CaO	4.75	4.13	2.77	3.49	3.44	13.27	14.10	14.99	11.06	7.22	4.45	3.95
Na_2O	8.86	9.05	10.01	9.59	9.76	3.72	2.58	2.92	5.28	7.41	9.10	9.21
K_2O	0.03	0.03	0.04	0.09	0.10	0.05	0.13	0.04	0.02	0.03	0.07	0.04
BaO	0.00	0.00	0.00	0.03	0.05	0.07	0.06	0.05	0.03	0.00	0.00	0.00
Total	99.09	99.15	99.80	99.29	99.16	100.80	99.40	100.61	100.36	100.02	100.00	99.91
Si	2.78	2.81	2.88	2.86	2.86	2.36	2.31	2.27	2.46	2.66	2.79	2.83
Al	1.21	1.20	1.12	1.13	1.13	1.63	1.68	1.72	1.53	1.34	1.21	1.17
Fe^{3+}	0.00	0.00	0.00	0.00	0.00	0.02	0.03	0.02	0.01	0.01	0.00	0.01
Ca	0.23	0.20	0.13	0.17	0.16	0.64	0.69	0.73	0.53	0.35	0.21	0.19
Na	0.77	0.78	0.86	0.83	0.84	0.33	0.23	0.26	0.46	0.64	0.78	0.79
K	0.00	0.00	0.00	0.01	0.01	0.00	0.01	0.00	0.00	0.00	0.00	0.00
Ba	0.00	0.00	0.00	0.00	0.00	0.00	0.00	0.00	0.00	0.00	0.00	0.00
Total	4.99	4.98	4.99	4.99	5.00	4.98	4.95	4.99	5.00	4.99	5.00	4.99
X_{Ab}	0.77	0.80	0.87	0.83	0.83	0.34	0.25	0.26	0.46	0.65	0.79	0.81
X_{An}	0.23	0.20	0.13	0.17	0.16	0.66	0.75	0.74	0.54	0.35	0.21	0.19
X_{Or}	0.00	0.00	0.00	0.01	0.01	0.00	0.01	0.00	0.00	0.00	0.00	0.00

Cations calculated on the basis of 8 oxygen; inc. = inclusions in Grt and cor. = corona. sym. 1 = symplectite between Grt and Ky; sym. 2 = symplectite between Grt and Omp.

Table 6
Representative electron microprobe analyses of staurolite and spinel of retrograde sympletites, zoisite and hornblende of the kyanite-bearing eclogites.

Sample	T125-1-04 Staurolite			Spinel			Zoisite			Hornblende				
No.	19 sy.	20 sy.	21 sy.	377 sy.	378 sy.	381 sy.	206 rim	209 core	212 core	16 sy.	104 sy.	227 mt.	228 mt.	229 mt.
SiO_2	25.21	25.16	25.13	0.07	0.09	0.12	38.95	39.79	39.73	40.28	39.57	40.37	40.41	40.80
TiO_2	0.24	0.12	0.13	0.00	0.01	0.00	0.29	0.13	0.17	0.74	0.69	0.40	0.43	0.50
Al_2O_3	56.98	57.01	57.08	58.94	59.24	61.17	26.36	30.86	30.76	16.20	16.54	15.13	15.34	14.86
Cr_2O_3	0.00	0.00	0.00	0.00	0.03	0.01	0.13	0.01	0.04	0.04	0.00	0.00	0.03	0.02
FeO	13.05	13.04	13.03	26.22	26.21	26.05	6.65	0.86	0.50	14.78	16.47	15.40	15.28	15.31
Fe_2O_3	0.00	0.00	0.00	3.80	3.01	0.00	1.85	2.31	2.32	0.00	0.00	0.00	0.00	0.00
MgO	3.27	3.27	3.29	9.48	9.42	8.25	0.26	0.12	0.11	10.21	9.31	10.32	10.08	10.22
MnO	0.00	0.02	0.01	0.17	0.24	0.17	0.07	0.04	0.03	0.19	0.18	0.25	0.37	0.38
CaO	0.29	0.28	0.36	0.09	0.08	0.06	22.74	22.83	22.97	11.42	11.36	11.71	11.56	11.38
Na_2O	0.00	0.00	0.00	0.00	0.00	0.00	0.02	0.07	0.05	2.91	2.86	2.86	2.83	2.81
K_2O	0.00	0.00	0.00	0.00	0.00	0.00	0.00	0.02	0.00	0.16	0.47	0.15	0.15	0.16
ZnO	0.04	0.07	0.08	–	–	–	–	–	–					
Total	99.08	98.95	99.10	98.77	98.33	95.84	97.31	97.05	96.67	96.93	97.45	96.59	96.47	96.43
Si	7.22	7.21	7.20	0.02	0.02	0.03	3.06	3.07	3.08	6.04	5.97	6.11	6.12	6.17
Ti	0.05	0.03	0.03	0.00	0.00	0.00	0.02	0.01	0.01	0.08	0.08	0.05	0.05	0.06
Al	19.24	19.27	19.28	15.34	15.45	16.17	2.44	2.81	2.81	2.87	2.94	2.70	2.74	2.65
Cr	0.00	0.00	0.00	0.00	0.00	0.00	0.01	0.00	0.00	0.00	0.00	0.00	0.00	0.00
Fe^{2+}	3.13	3.13	3.12	4.84	4.85	4.89	0.12	0.15	0.15	1.85	2.08	1.95	1.93	1.94
Fe^{3+}	0.00	0.00	0.00	0.63	0.50	0.00	0.39	0.05	0.03	0.00	0.00	0.00	0.00	0.00
Mg	1.40	1.40	1.40	3.12	3.11	2.76	0.03	0.01	0.01	2.28	2.09	2.33	2.27	2.31
Mn	0.07	0.07	0.09	0.03	0.04	0.03	0.00	0.00	0.00	0.02	0.02	0.03	0.05	0.05
Ca	0.00	0.00	0.00	0.02	0.02	0.01	1.92	1.89	1.91	1.84	1.84	1.90	1.87	1.84
Na	0.00	0.00	0.00	0.00	0.00	0.00	0.00	0.01	0.01	0.85	0.84	0.84	0.83	0.82
K	0.00	0.00	0.00	0.00	0.00	0.00	0.00	0.00	0.00	0.03	0.09	0.03	0.03	0.03
Zn	0.01	0.01	0.02	–	–	–	–	–	–	–	–	–	–	–
Total	31.11	31.12	31.13	24.00	24.00	23.89	8.00	8.00	8.00	15.88	15.95	15.93	15.89	15.87
X_{Mg}	0.31	0.31	0.31	0.39	0.39	0.36				0.55	0.50	0.54	0.54	0.54

Cations calculated on the basis of 48 oxygen for St, 12.5 for Zo, 23 for Hbl and 32 for Spl; sy. = symplectite; mt. = matrix.

temperature conditions experienced during subduction (Fig. 4B). The chemistry of the mineral inclusions (Ab_{85}–Jd_{10}–Qz) results in prograde pressures that are very similar to those calculated from inclusions found in kyanite of the kyanite-bearing eclogites (Fig. 6). However, temperature estimates using the Fe–Mg exchange between garnet and the included omphacite result in very high temperatures of 930–940 °C which is not regarded as realistic. Two additional samples gave slightly lower temperatures of 760–790 °C and 850–890 °C depending on the calibration applied (Table 7; T108-7-04 and T121-3-04). In order to get more data on temperature estimates we also applied the Zr-in-rutile thermometer. The temperature dependence of Zr substitution in rutile has great potential for geothermometry in metabasites (e.g. Spear et al., 2006). The Zr-in-rutile thermometer calibrations of Watson et al. (2006), Tomkins et al. (2007) and Ferry and Watson (2007) were applied. Matrix rutile and rutile included in garnet and omphacite of three samples have similar Zr content and the grains are unzoned. This results in similar temperatures for these kyanite-free eclogite samples (Table 7 and Fig. 7). The calibration of Watson et al. (2006) and Ferry and Watson (2007) yield similar average temperatures, which range between 610 °C and 650 °C. However, the calibration of Tomkins et al. (2007) gives slightly higher average temperatures between 650 °C and 690 °C (Table 7), which is still about 200 °C lower than the results from garnet–clinopyroxene Fe–Mg exchange thermometry on the same samples (Table 7; Fig. 6). If we combine the Zr-in-rutile temperatures of 610–690 °C with pressure calculations from inclusions (Ab–Jd–Qz) we obtain pressure at 16–17 kbar (Fig. 6B). A further temperature increase to possible higher peak pressures and temperatures seems not to be recorded in rutile grains of the matrix, as matrix rutile has similar Zr contents as rutile inclusions. This may indicate that rutile became included near the peak temperature, when burial by subduction was still going on. Peak pressures cannot be calculated for the kyanite-free eclogites as plagioclase was not stable in the matrix, but was only found as relic grains as inclusions in garnet. If we take the values of 20 kbar/785 °C (THERMOCALC) and 20 kbar/690 °C (rutile thermometry) as the peak metamorphic conditions of the eclogites, we obtain geothermal gradients in the corresponding subduction zone in the range of 10–11 °C/km, indicating a relatively warm subducted slab.

7. Geochemistry of kyanite-free eclogites

A total of 12 samples of the kyanite-free eclogites from the Chisi area were selected for major and trace element analyses; results are given in Table 8. SiO_2-contents range between 45.8 and 51.9 wt.% and the ratios Nb/Y (0.07–0.95) and Zr/Ti (0.01–0.07) are similar to those of tholeiitic basalts (Fig. 8). Our eclogite samples display the FeO–TiO_2 enrichment which is a characteristic of MORB tholeiite glasses (Fig. 8B). The concentration of K_2O in different samples is very low ranging between 0.01 and 0.07 (Table 8; see Footnote 1), which is in agreement with an interpretation that the precursor rocks have been low-K (tholeiitic) basalts. However, the concentrations of large ion lithophile elements (LILEs) such as Na_2O and K_2O can only be used in a semi-quantitavely way because of their mobility during metamorphism (e.g., Tatsumi et al., 1986). Tholeiitic magmas are known to erupt in different tectonic settings such as MOR (mid oceanic ridges), island-arcs, oceanic islands and in continental rifts (Pearce and Cann, 1973). Tholeiitic basalts from these diverse tectonic settings can be distinguished on the basis of their distinctive rare earth and other trace element concentrations and ratios, e.g. Pearce and Cann (1973), Sun and McDonough (1989) and John et al. (2003).

On the basis of the chondrite-normalized rare earth elements (REEs) the kyanite-free eclogites were divided into two groups: the first group (group I) has light rare earth elements (LREEs) 10–30 times chondritic values, and the second group (group II) has LREE contents 30–80 times chondritic values (Fig. 9A and C). The

Table 7
A summary of pressure and temperature estimates of the kyanite-bearing and kyanite-free eclogites. For thermobarometry Fe^{3+} of pyroxene has been calculated assuming stoichiometry. Abbreviations for minerals is according to Whitney and Evans (2010).

Sample no.	Mineral and analysis no.	Calibration	T (°C)	P (kbar)	Remarks
Fe–Mg exchange in Grt–Cpx and Grt–Hbl geothermometers					
T108-7	Grt_{91}–Cpx_{79}	Ellis and Green (1979)	850	17[a]	Grt–Cpx cores
		Powell (1985)	890	17[a]	Grt-Cpx cores
T121-3	Grt_{59}–Cpx_{15}	Ellis and Green (1979)	760	17[a]	Grt–Cpx cores
		Powell (1985)	790	17[a]	Grt–Cpx cores
T111-5	Grt_{202}–Cpx_{176}	Ellis and Green (1979)	930	17[a]	Grt–Cpx cores
		Powell (1985)	940	17[a]	Grt–Cpx cores
T111-5	Grt_{28}–Hbl_{13}	Graham and Powell (1984)	710	12[e]	Hbl corona and Grt rim
T125-2	Grt_{265}–Hbl_{16}	Graham and Powell (1984)	740	10[b]	Hbl symp. and Grt rim
Ab = Jd + Qtz and GASP geobarometers					
T111-1	Cpx_{176}–Pl_{157}	Holland (1980)	700[a]	17	Inclusion in Grt
T111-5	Cpx_{95}–Pl_{53}	Holland (1980)	710[c]	12	Symplectites
T125-4	Cpx_{80}–Pl_{84}	Holland (1980)	715[d]	16	Pl inclusion in ky
T125-4	Grt_{98}–Pl_{90}	Koziol (1989)	715[d]	16	Inclusion in Ky
T125-1	Grt_{523}–Pl_{290}	Koziol (1989)	785[d]	20	Grt-Pl cores
T125-2	Grt_{265}–Hbl_{16}–Pl_{26}	Kohn and Spear (1990)	740[c]	10	Hbl-Pl symp.
THERMOCALC					
T125-4	Grt_{290}–Cpx_{160}–Pl_{31}–Zo_{210}	Holland and Powell (1998)	785 ± 81	20.1 ± 3.4	Peak P–T
	Grt_{19}–Cpx_{80}–Pl_{109}	Holland and Powell (1998)	715 ± 108	15.5 ± 3.0	Inclusion in Ky
	Grt_{298}–St_{20}–Spl_{377}–Pl_{395}	Holland and Powell (1998)	700 ± 131	11.0 ± 3.5	Symp. and Grt rim

Zr-in-rutile thermometry of Ky-free eclogites

Sample	Grain	No. of spots	Mean Zr (ppm) error at 1σ	Mean (T °C) error at 1σ		
				W	T[f]	FW
T108-7-04	Rt-1 inclusion in Omp	30	312 ± 15	646 ± 4	683 ± 4	641 ± 4
	Rt-2 matrix	25	299 ± 21	642 ± 8	679 ± 8	637 ± 4
	Rt-3 inclusion in Grt	20	312 ± 6	646 ± 4	683 ± 4	641 ± 4
T111-5-04	Rt-1 inclusion in Omp	30	300 ± 17	642 ± 5	680 ± 5	638 ± 5
	Rt-2 matrix	20	316 ± 24	647 ± 7	684 ± 7	642 ± 6
	Rt-3 inclusion in Grt	20	282 ± 12	637 ± 4	675 ± 4	633 ± 3
T121-3-04	Rt-1 matrix	30	227 ± 14	620 ± 5	657 ± 5	616 ± 4
	Rt-2 inclusion in Grt	20	207 ± 8	613 ± 4	650 ± 4	609 ± 3

Note: Analysis numbers correspond to tables. For Zr-in-rutile thermometry: W = Watson et al. (2006), T = Tomkins et al. (2007) and FW = Ferry and Watson (2007).
[a] Inferred temperature or pressure.
[b] Grt–Pl–Hbl geobaometry (Kohn and Spear, 1990).
[c] Grt–Hbl thermometry (Graham and Powell, 1984).
[d] THERMOCALC (Holland and Powell, 1998).
[e] Cpx-Pl-Qtz geobaometry (Kohn and Spear, 1990); symp. = symplectite; incl. = inclusion.
[f] Temperatures were calculated at a reference peak pressure of 17 kbar.

chondrite-normalized REE patterns of group I is generally similar to the average N-MORB. However, the heavy rare earth elements (HREEs) lie below the average N-MORB pattern, which is true for group II eclogites as well. There is a Ce anomaly in some samples from both groups. The Ce anomaly may be caused by interaction of eclogite precursor basalts with sea-water (e.g. Neal and Taylor, 1989). The MORB-normalized REEs and high field strength elements (HFSEs) concentrations of group I eclogites plot parallel to MORB values, with minor deviations. However, the fluid-mobile elements like U, Ba and sometimes Rb and Cs, are enriched or depleted, up to about ten fold relative to their concentration of MORB (Fig. 9B). Th, one of the HFSEs, which are fluid immobile and incompatible, is slightly enriched relative to MORB. The Th enrichment could reflect the addition of a melt component from a subducting slab with a low degree of partial melting (e.g. Kelemen et al., 2003). Generally the REEs and HFSEs patterns of group I eclogites point to a composition similar to melts from a MORB source region.

The MORB-normalized trace element patterns of group II eclogites are strikingly similar to the average composition of primitive island-arc tholeiite basalt (Fig. 9D). The Nb–Ta depletion relative to the LREEs and LILEs, which is a typical arc signature, is evident in all samples of group II eclogites. Zr and Hf are depleted relative to Nd and Sm; Ti is depleted relative to Eu and Gd. Mismatch of the patterns is only seen for the easily mobilized elements Cs and Rb, which show depletion. In group II eclogites, Th is more enriched (ranging between 5 and 40 times MORB values) than in group I eclogites. Th enrichment in basalts might reflect a partial melt component of eclogite facies basalt and/or sediment in arc-magmas (as discussed above), which might be precursors of the group II eclogites.

The assemblage of rock suits with MORB signature (group I eclogites) and volcanic-arc basalt signature (group II eclogites) can be explained by a model that involves a marginal oceanic basin, of which back-arc basalts and oceanic-arc basalts were subducted. Back-arc spreading settings at their advanced evolution stage produce basalts with geochemical composition similar to basalts that form at mid ocean ridges in large ocean basins (e.g. Clift, 1995; Hawkins, 1995). Therefore, precursor melts of the group I eclogites probably were generated in an evolved back-arc setting.

8. Geochronology

8.1. Textures and U–Th–Pb compositions of zircon

Rounded and subrounded zircon grains were selected from two kyanite-free eclogite samples (T111-5 and T108-7) and one kyanite-bearing eclogite sample (T125-3) for geochronology (Fig. 10). The analytical results are presented in Table 9 (see Footnote 1) and Fig. 11. Cathodoluminescence (CL) images reveal that

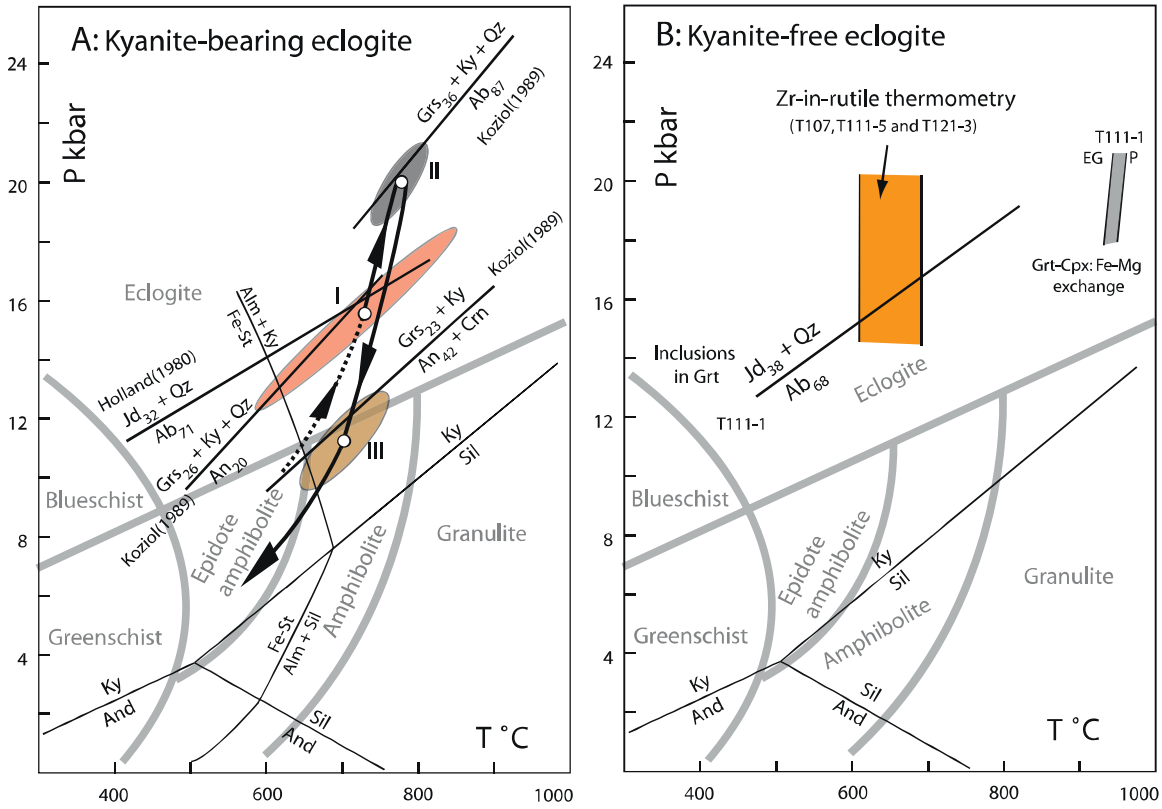


Fig. 6. (A) The subduction *P*–*T* path of the Ky-bearing eclogites of the Ufipa Terrane. The circles in the error ellipses labeled I, II and III mark the average *P*–*T* values calculated by using the THERMOCALC program (Holland and Powell, 1998). Ellipse I indicates the prograde average $P = 15.5$ kbar and $T = 715$ °C constrained by using the Grt–Omp–Pl–Qz inclusions in Ky. Ellipse II shows the peak average *P*–*T* values of $P = 20$ kbar and $P = 785$ °C calculated by using the peak mineral assemblage Grt–Ky–Zo–Pl–Qz. Ellipse III shows the retrograde average *P*–*T* values $P = 11$ kbar and $T = 700$ °C calculated by using the Crn–Pl–Spl–St symplectites and the rim of Grt corona. Other geothermobarometers give similar *P*–*T* conditions as the average *P*–*T* esimates; the GASP and Ab = Jd + Qz equilibria. The Fe–St out reaction is from Spear and Cheney (1989). (B) *P*–*T* estimates for the kyanite-free eclogites. Zr-in-rutile thermometers (Watson et al., 2006; Tomkins et al., 2007; Ferry and Watson, 2007) give temperatures of 610–690 °C, which correspond to peak pressures at 15–17 kbar estimated by using the Ab = Jd + Qz equilibrium of Holland (1980). Fe–Mg exchange (garnet–clinopyroxene) thermomters EG = Ellis and Green (1979) and P = Powell (1985) give higher temperatures than Zr-in-rutile thermometers.

zoned zircon grains occur in all samples (Fig. 10). Kyanite-free eclogites contain zircon grains with uniform composition displaying no zones (Fig. 10A), and zircon grains with rims around cores (Fig. 10B). Zircon from the kyanite-bearing eclogite have rims, which surround a core and a mantle that are characterized by oscillatory growth zoning (Fig. 10C). Oscillatory growth zoning texture

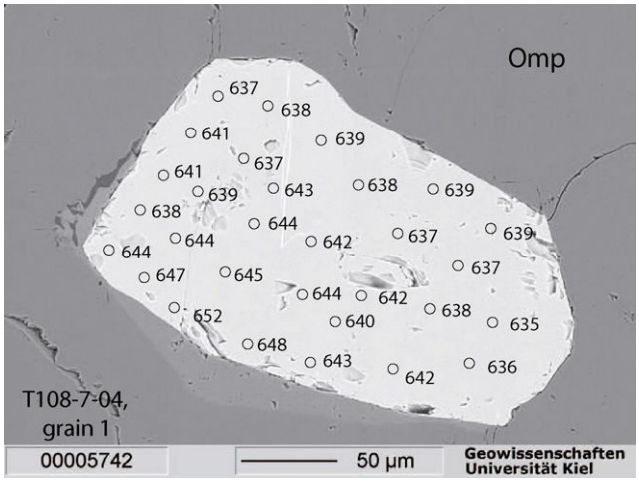


Fig. 7. Backscattered electron image of rutile crystal from sample T108-7-04. Circles show location of analysis points. Numbers are temperatures in °C calculated from rutile thermometer (calibration of Ferry and Watson, 2007).

in cores of these zircon grains is considered to have developed during magmatic crystallization of the eclogite precursor, because this kind of texture is characteristic for magmatic zircon (e.g. Corfu et al., 2003)

The cores and rims of zircon grains from the kyanite-free eclogites have U contents (34–161 ppm) and Th contents (3–59 ppm), which give overlapping low Th/U values that range between 0.09 and 0.37 (Table 9; see Footnote 1). The absence of concentric growth zoning in these zircon grains and the low Th/U may indicate growth of both the cores and rims during metamorphism (Rubatto, 2002; Corfu et al., 2003).

Th/U of zircon cores in the kyanite-bearing eclogite overlap with those of the mantles (ranging from 0.24 to 1.72). Data from the outer rims of these zircon grains plot randomly in the concordia diagram and no meaningful ages can be calculated from them, therefore these analyses are not considered here.

8.2. U–Pb dating results

The core and rim analyses of zircon grains of the kyanite-free eclogites plot together on the U–Pb concordia, for which a concordant age of 593 ± 20 Ma for sample T111-5 was calculated (Fig. 11A). A concordant age of 524 ± 12 Ma was obtained from core and rim analyses of sample T108-7 (Fig. 11B).

Data points of zircon core and mantle of the kyanite-bearing eclogite sample T125-3 plot at variable degree of discordance ranging between 3 and 88% (Table 9; see Footnote 1). The oscillatory-zoned zircon core data points form a discordia, with

Table 8
Major and trace element composition of the kyanite-free eclogites of the Ufipa Terrane.

	T111-5	T109-2	T123-2	T124-2	T121-1	T123-1	T129-1	T108-4	T110-1	T110-2	T112-4	T121-3
	Group I eclogites				Group II eclogites							
Major elements in wt%												
SiO_2	45.96	46.87	48.65	51.27	51.34	51.86	48.60	47.32	47.41	46.88	45.81	45.96
TiO_2	1.56	1.70	1.09	1.79	2.15	1.07	1.25	1.09	1.46	1.44	5.22	1.08
Al_2O_3	15.67	16.13	14.37	13.48	14.16	14.80	7.15	15.84	14.64	14.84	10.79	13.68
FeO	13.93	14.56	12.04	13.23	13.33	11.40	17.64	13.01	12.99	13.06	11.27	15.55
MnO	0.24	0.24	0.29	0.21	0.21	0.16	0.25	0.24	0.22	0.22	0.20	0.23
MgO	10.58	7.04	9.80	6.33	5.88	6.46	14.38	8.74	9.85	10.10	9.19	9.51
CaO	9.16	9.88	10.05	10.39	9.55	9.51	9.40	9.44	9.21	9.47	13.85	12.07
Na_2O	2.73	3.27	3.86	3.27	3.22	4.88	1.51	3.59	3.70	3.43	3.03	2.00
K_2O	0.06	0.05	0.01	0.01	0.04	0.07	0.03	0.02	0.01	0.01	0.03	0.01
P_2O_5	0.19	0.17	0.16	0.18	0.03	0.02	0.18	0.05	0.19	0.27	0.58	0.02
LOI	0.00	0.00	0.00	0.00	0.00	0.00	0.00	0.00	0.00	0.00	0.00	0.00
Total	100.08	99.91	100.32	100.16	99.91	100.23	100.39	99.34	99.68	99.72	99.97	100.11
Trace elements in ppm												
Zr	126	117	92	134	139	63	74	91	124	121	296	39
Li	8.50	14.7	14.0	19.0	13.2	8.08	8.25	17.4	9.83	8.48	9.90	11.1
Sc	42.7	38.8	32.8	46.3	52.0	37.1	67.1	35.1	38.4	37.5	36.0	49.7
V	257	305	252	342	330	319	338	249	257	248	354	465
Co	68.6	46.3	51.7	46.1	49.6	40.7	92.3	56.5	57.4	57.8	43.4	64.0
Ni	275	91.7	278	61.2	68.2	112	219	207	257	244	128	140
Cu	38.5	46.4	21.8	43.4	388	108	114	207	23.5	27.8	111	777
Zn	147	140	110	129	141	118	148	157	141	141	147	102
Ga	16.0	19.6	17.3	19.4	20.8	20.0	10.0	17.6	16.8	16.2	20.9	18.7
Rb	2.25	0.758	0.22	0.271	1.03	0.867	0.791	0.530	0.338	0.243	1.66	0.261
Sr	117	83.3	103	92.2	190	168	184	152	104	222	318	153
Y	31.4	37.2	22.2	29.4	30.6	29.1	21.0	29.7	30.4	31.4	27.5	23.6
Zr	126	97.4	76.7	103	103	45.7	65.9	75.5	97.6	96.6	244	21.6
Nb	9.70	8.01	9.74	5.39	12.70	14.50	6.66	4.06	7.70	7.00	132	1.58
Cs	0.039	0.003	0.008	0.010	0.023	0.006	0.034	0.018	0.006	0.004	0.025	0.007
Ba	101	17.6	226	12.3	71.2	55.2	243	206	246	336	314	374
La	3.63	8.23	8.26	8.22	18.9	20.5	17.6	12.0	9.34	13.7	16.3	14.2
Ce	10.9	15.7	12.8	10.2	35.5	25.5	39.9	21.1	21.6	26.7	30.4	31.7
Pr	1.82	3.30	2.34	2.47	4.30	5.41	5.59	2.89	3.37	4.16	4.96	4.41
Nd	9.62	16.6	10.8	11.7	16.9	22.3	24.0	13.2	16.0	19.0	21.7	19.7
Sm	3.63	6.19	3.51	3.88	4.67	6.45	5.74	4.09	4.77	5.36	5.20	5.53
Eu	1.29	2.05	1.07	1.44	1.56	1.65	1.41	1.51	1.59	1.76	1.73	1.51
Gd	4.61	8.15	4.39	5.14	5.05	6.91	5.37	5.14	5.52	6.04	6.20	5.68
Tb	0.84	1.33	0.73	0.86	0.84	1.11	0.78	0.85	0.91	0.97	1.05	0.87
Dy	5.11	7.55	4.31	5.43	5.05	6.15	4.34	5.29	5.59	5.82	6.08	4.59
Ho	1.04	1.40	0.83	1.13	1.04	1.11	0.81	1.08	1.14	1.17	1.09	0.81
Er	2.94	3.52	2.18	3.05	2.92	2.79	2.07	2.91	3.14	3.16	2.57	2.07
Tm	0.422	0.497	0.325	0.459	0.408	0.398	0.284	0.423	0.473	0.464	0.325	0.291
Yb	2.67	3.19	2.15	3.05	2.56	2.61	1.75	2.74	3.10	3.01	1.94	1.89
Lu	0.394	0.457	0.327	0.452	0.382	0.376	0.239	0.409	0.451	0.441	0.259	0.272
Hf	2.90	2.73	2.04	2.96	2.81	1.74	1.97	2.05	2.61	2.55	6.74	0.835
Ta	0.427	0.320	0.535	0.363	0.585	0.585	0.263	0.235	0.445	0.423	6.80	0.052
Pb	6.89	3.75	3.83	5.15	22.2	14.7	115.0	22.8	8.5	14.4	13.7	21.0
Th	0.335	0.130	0.644	0.463	3.86	2.14	1.41	1.87	0.86	1.09	0.677	1.58
U	0.334	0.841	0.488	0.443	0.902	0.964	3.00	0.377	0.469	0.447	0.949	1.02

LOI, loss on ignition.

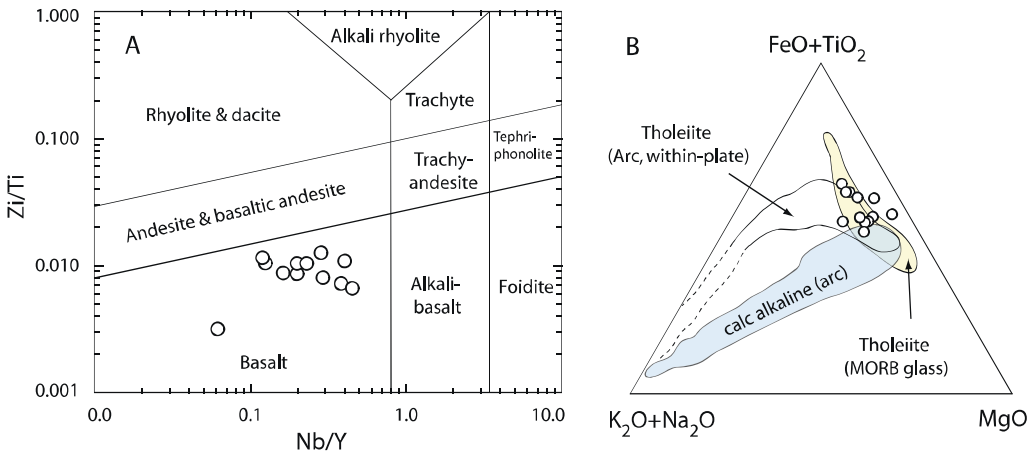


Fig. 8. (A) Magma series discrimination diagram after Pearce (1996): the kyanite-free eclogites plot in the basalt field. (B) The eclogites show the MORB Fe-enrichment trend in the AFM diagram, similar to MORB.

Table 9
U–Pb isotopic zircon composition for the kyanite-free and kyanite-bearing eclogites of the Ufipa Terrane.

Spot	U (ppm)	Th (ppm)	Th/U	$^{206}Pb^a$ (ppm)	$^{206}Pb_c$ (%)	Age (Ma)				Isotopic ratios						
						$^{207}Pb/^{206}Pb$	±	$^{206}Pb/^{238}U$	±	$^{207}Pb^a/^{206}Pb^a$	±(%)	$^{206}Pb^a/^{238}U$	±(%)	$^{207}Pb^a/^{235}U$	±(%)	Disc.[b] (%)
T111-5																
Rim																
1.2	130	23	0.18	11.00	0.59	573	110	602	21	0.059	5.0	0.098	3.6	0.799	6.2	0
2.1	34	3	0.09	2.91	1.56	360	330	601	23	0.054	15.0	0.098	4.0	0.720	15.0	0
3.1	37	9	0.25	3.00	2.39	450	380	568	22	0.056	17.0	0.092	4.0	0.710	18.0	0
Core																
1.1	34	5	0.15	2.92	0.97	729	290	615	24	0.064	14.0	0.100	4.1	0.880	14.0	0
3.2	35	3	0.09	2.88	1.62	374	470	585	23	0.054	21.0	0.095	4.1	0.710	21.0	0
T108-7																
Rim																
1.2	75	22	0.29	6.19	0.54	556	150	586	21	0.059	7.0	0.095	3.7	0.771	7.9	0
2.1	137	48	0.35	10.40	1.14	307	400	541	17	0.053	18.0	0.088	3.2	0.630	18.0	0
3.1	98	36	0.37	6.97	0.85	396	220	507	15	0.055	9.8	0.082	3.0	0.616	10.0	0
4.1	77	23	0.29	5.43	1.12	612	190	505	14	0.060	8.8	0.082	2.9	0.677	9.3	0
Core																
1.1	78	22	0.28	6.29	0.93	514	210	570	20	0.058	9.4	0.092	3.7	0.733	10.0	0
2.2	130	37	0.29	7.63	0.00	308	160	427	13	0.053	7.2	0.068	3.1	0.495	7.8	0
4.2	161	59	0.37	11.60	0.28	528	97	517	14	0.058	4.4	0.084	2.8	0.668	5.2	0
4.3	99	30	0.30	6.90	0.56	528	110	503	14	0.058	4.8	0.081	2.8	0.648	5.6	0
T125-3																
Mantle																
1.2	48	80	1.65	10.20	0.00	1739	110	1415	46	0.106	5.9	0.245	3.6	3.600	6.9	43
2.2	90	120	1.34	20.40	2.71	1273	300	1478	39	0.083	15.0	0.258	2.9	2.950	15.0	56
4.2	131	151	1.15	38.30	0.36	1897	56	1881	34	0.116	3.1	0.339	2.1	5.420	3.7	7
7.1	348	254	0.73	83.20	0.12	1770	29	1580	13	0.108	1.6	0.278	0.9	4.146	1.9	32
8.2	50	87	1.72	14.80	1.17	1770	120	1869	37	0.108	6.5	0.336	2.3	5.020	6.9	15
9.2	34	45	1.32	9.70	0.39	1853	90	1859	59	0.113	5.0	0.334	3.6	5.220	6.2	11
10.2	41	65	1.59	13.00	1.16	1850	110	2000	88	0.113	6.2	0.364	5.1	5.670	8.1	3
Core																
1.1	216	214	0.99	27.00	2.19	1108	220	859	51	0.077	11.0	0.143	6.4	1.500	13.0	84
2.1	170	218	1.28	42.90	0.38	1715	61	1651	26	0.105	3.3	0.292	1.8	4.230	3.8	31
4.1	212	140	0.66	41.80	0.00	1758	45	1333	18	0.108	2.5	0.230	1.5	3.407	2.9	47
8.1	295	72	0.24	30.80	0.27	1152	72	738	76	0.078	3.6	0.121	1.1	1.308	3.8	88
9.1	137	126	0.92	30.50	0.65	1736	71	1481	22	0.106	3.8	0.258	1.7	3.780	4.2	40
10.1	329	309	0.94	56.90	0.81	1427	100	1173	15	0.090	5.3	0.200	1.4	2.480	5.5	65

Pb^c and Pb^a indicate the common and radiogenic portions, respectively.

[a] Common Pb corrected using measured ^{204}Pb. Age errors are given as 1-sigma.

[b] Discordance of results expressed as a distance of a data point along a discordia measured from the upper interecept towards the lower intercept.

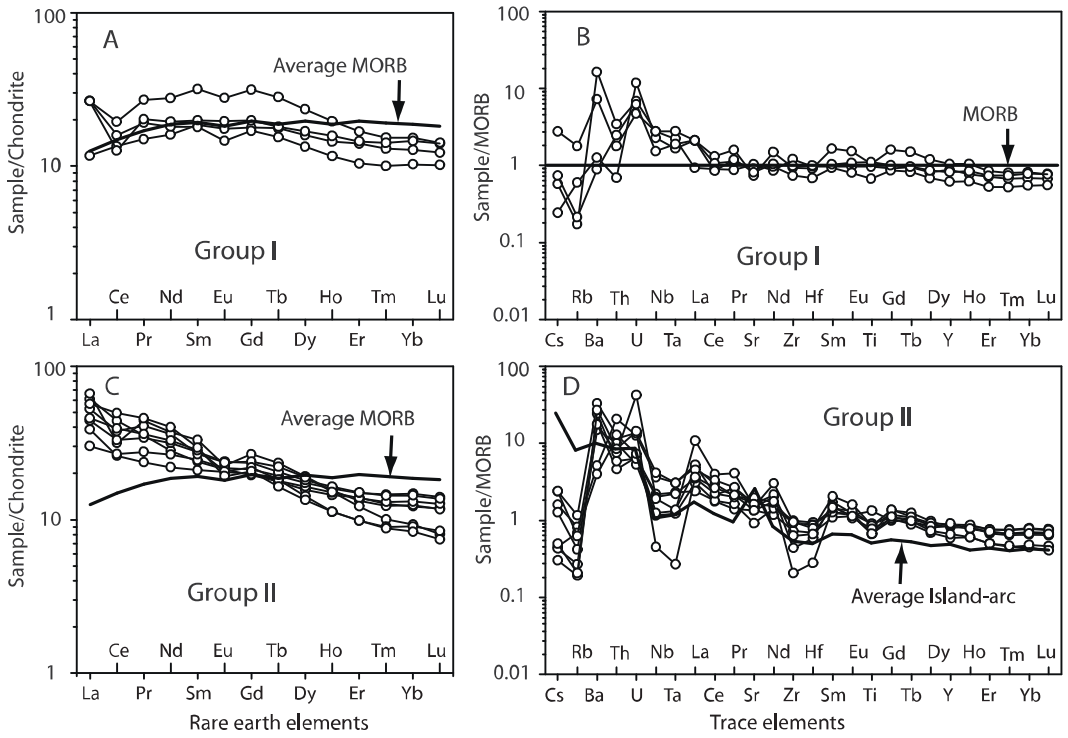


Fig. 9. Trace element patterns of kyanite-free eclogites. (A) Chondrite-normalized REE patterns of group I eclogites; chondrite values are from (Boynton, 1984). (B) MORB-normalized trace element patterns of group I eclogites; MORB normalizing values are from (Hofmann, 1988). (C) Chondrite-normalized REE patterns of group II eclogites. (D) MORB normalized trace element patterns of group II eclogites. The average trace element concentration of island-arc basalts is from Kelemen et al. (2003).

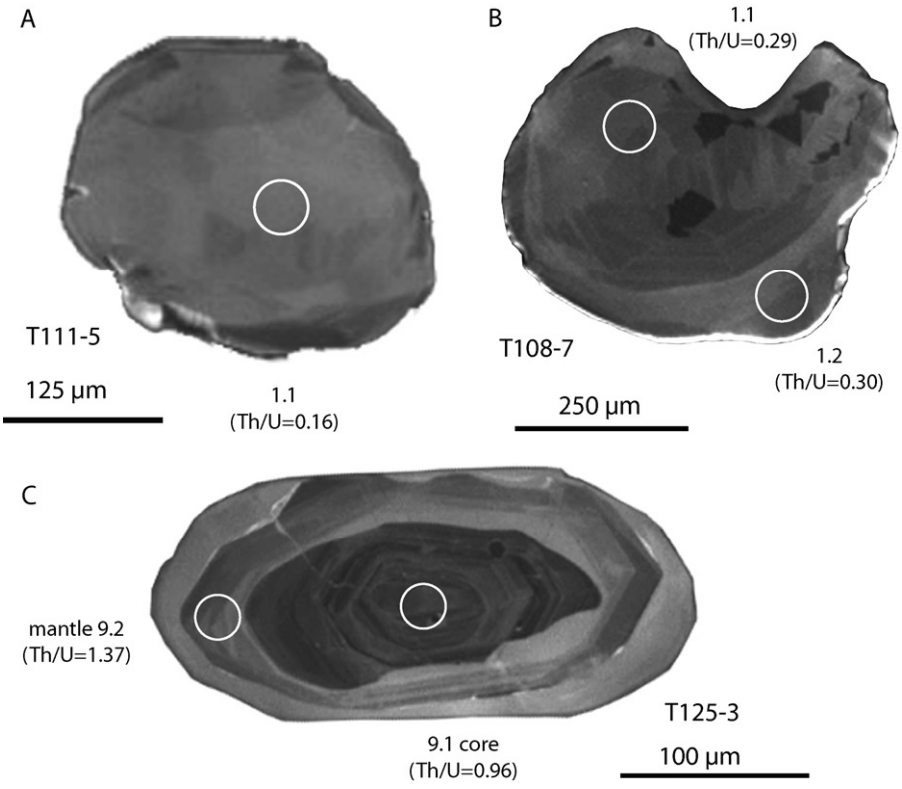


Fig. 10. CL images showing textures and Th/U values of zircon grains of Pan-African eclogites of the Ubendian Belt. (A) Metamorphic zircon of a kyanite-free eclogite without magmatic cores. (B) Zircon of a kyanite-free eclogite with cores and rims that have similar Th/U. (C) Zircon of a kyanite-bearing eclogite, of which core and mantle with magmatic growth zones are surrounded by a rim.

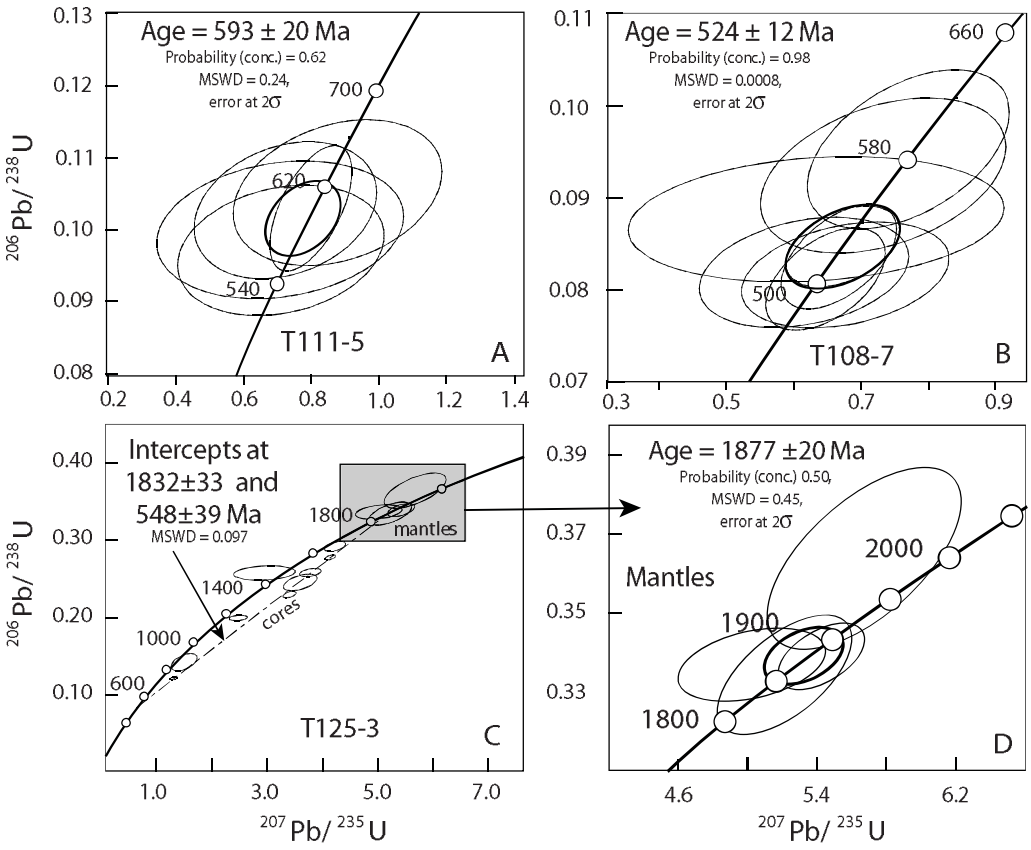


Fig. 11. Concordia diagrams of Ufipa Terrane eclogites. (A and B) Two samples of the kyanite-free eclogites. Zircon cores and rims give concordant Pan-African ages. (C) Zircon cores of the kyanite–eclogite plot along a discordia with intercepts at 1832 ± 33 and 548 ± 39 Ma whereas the mantles plot concordantly at 1877 ± 20, this age is clearly illustrated in diagram (C).

an upper intercept at 1832 ± 33 Ma and a lower intercept at 548 ± 39 Ma (Fig. 11C). The nearly concordant data points of the zircon mantles (disc. 3–15%) yield a concordant age at 1877 ± 20 Ma, which is equivalent to the above calculated upper intercept age from cores of zircon (Fig. 11C and D). The lower intercept age of the discordia discussed above points to a metamorphic event that is coeval with the concordant Pan-African ages of the kyanite-free eclogites.

The U–Pb zircon ages at 593 ± 20 and 524 ± 12 Ma from the kyanite-free eclogites have a difference of about 70 Ma. The time interval of this much long is not likely to represent a single subduction event. Therefore, it is more likely that successive accretions of volcanic-arc rocks occurred at 593 ± 20, 548 ± 39 and 524 ± 12 Ma.

9. Discussion and conclusions

9.1. Age, origin and nature of the Ufipa Terrane eclogites

The Pan-African U–Pb SHRIMP zircon ages of 593 ± 20, 548 ± 39 and 524 ± 12 Ma, obtained from the Ufipa Terrane eclogites is a surprising result. These eclogites were assumed by previous authors to represent relics of a Paleoproterozoic Ubendian suture zone (e.g. Sklyarov et al., 1998), similar to the 2.0 Ga eclogites with MORB-like geochemistry in the neighboring Usagaran Belt (Möller et al., 1995). The trace element compositions of the two recognized geochemical groups of kyanite-free eclogites (group I and group II eclogites) indicate that they are relics of a subducted marginal ocean basin in which island-arc volcanic rocks were associated with back-arc basin lavas during Pan-African time. This conclusion is based on the striking similarities of group II eclogites to oceanic island-arc lavas, which are characterized by the depletion of the HFSEs (Zr, Nb, Hf, Zr and Ti) relative to LILEs and LREEs (Perfit et al., 1980; Kelemen et al., 2003) and the chemical composition of group I eclogites, which resemble basalt composition of the back-arc settings. The MORB-normalized REEs and HFSEs concentrations of these rocks plot parallel to MORB values, with minor deviations. Therefore, it can be concluded that during Pan-African time an ocean basin and a magmatic-arc separated the Tanzania Craton from the Bangweulu Block along the Ubendian Belt.

The precursors of the kyanite-bearing eclogite are clearly relics of the Paleoproterozoic aluminous metabasic rocks of the Ubendian orogenic cycle (1890–1820 Ma; Boniface et al., 2012). Later in Pan-African time at about 550 Ma these rocks were metamorphosed to eclogite facies in a subduction zone. This means that the Neoproterozoic subduction of an oceanic crust in the Ubendian Belt was associated with metamorphic reworking of the Paleoproterozoic rocks. The Pan-African overprint ages are further observed in the entire Terrane of Ubende (north of the Ufipa terrne, Fig. 2), in which Paleoproterozoic eclogites with MORB-like chemistry and the associated metapelites were strongly mylonitized or reactivated during this episode (Boniface et al., 2012).

9.2. Pan-African suture zone in the Ubendian Belt and geodynamic implications

The subducted Neoproterozoic island-arc and back-arc basin basalts in the Ubendian Belt traversed a clockwise *PT* path that climaxed at pressures of 15–20 kbar and temperatures of 610–790 °C, indicating a geothermal gradient of about 10–11 °C/km. This thermal gradient is slightly warmer than that inferred for the Pan-African Zambezi Belt subduction zone (≈8 °C/km; John et al., 2003).

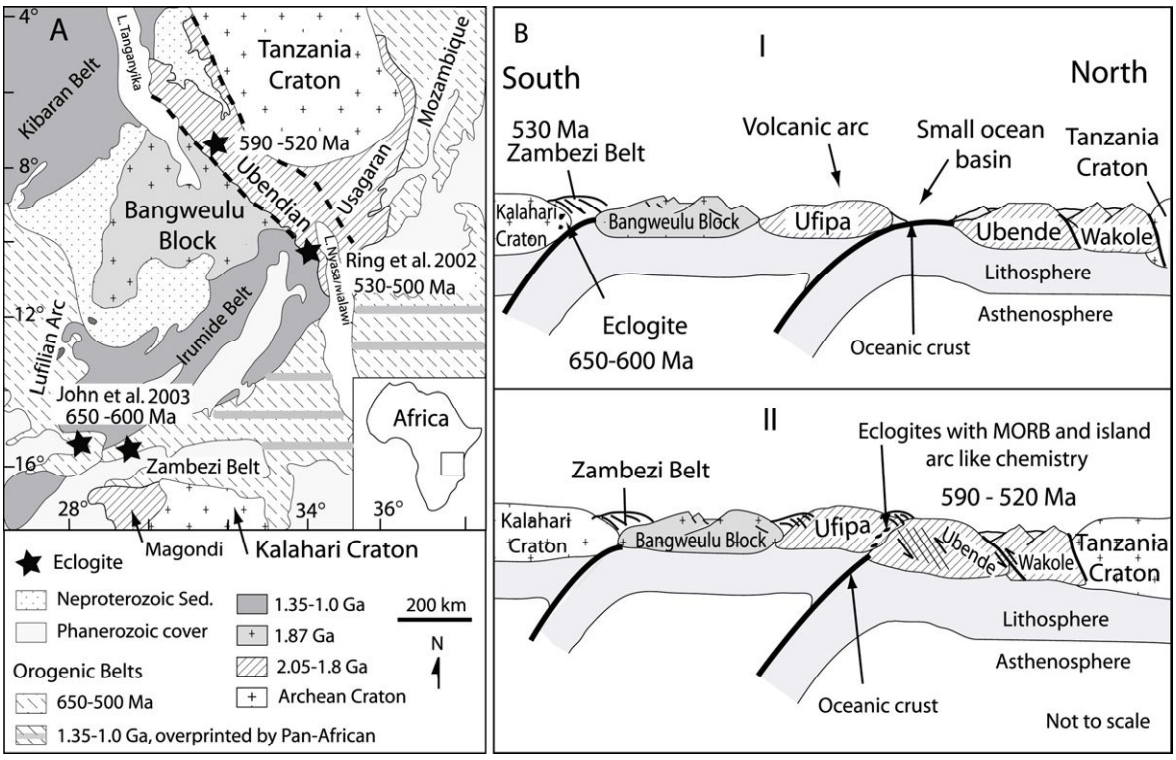


Fig. 12. (A) A geological map of southern central Africa indicating the location of Pan-African back-arc and island-arc like chemistry eclogites between the Bangweulu Block and the Tanzania Craton, the MORB-like chemistry eclogites of the Zambezi Belt (John et al., 2003) and the plume related Mozambique Belt eclogites in northern Malawi (Ring et al., 2002), a geological map was modified after from Hanson (2003). (B) A cartoon depicting a possible scenario of tectonic plates between the cratons of Congo and Kalahari during Pan-African time.

Rapid uplift resulted in a nearly isothermal decompression to amphibolite–facies conditions (about 10–12 kbar/700–740 °C), when abundant symplectites, coronas and sieve textured omphacites developed to replace eclogite peak mineral assemblages. Limited re-hydration favored the growth of hornblende and staurolite-bearing late-stage symplectites.

Several mechanisms and geological processes have been proposed to explain rapid uplift and exhumation of deep-seated high-pressure rocks: (1) erosion (e.g. Hsue, 1991; Nie et al., 1994), (2) large scale extensional collapse of a tectonically thickened continental crust (e.g. Burchfiel and Royden, 1985; Burchfiel et al., 1989), (3) arrival of a continent at the subduction zone, which produces stresses that promote the rise of the deeper parts of the subduction zone against the flow of subduction (Hynes et al., 1996), and (4) subduction channel processes, in which eclogites are exposed by buoyancy forces acting on the partially hydrated mantle wedge above a subducting slab (Gerya et al., 2002). One or more of these mechanisms might have been responsible for the uplift and exposure of the Pan-African eclogites in the Ubendian Belt.

In the search of possible information about the direction of subduction dip, we looked at the distribution of Neoproterozoic mineral assemblages in the metapelitic country rocks that host eclogites. The high-temperature mineral assemblages cordierite–garnet–sillimanite in the southeastern part of the Ufipa Terrane contrast with the kyanite–muscovite assemblages found along the northwestern border of the Ufipa Terrane, where the eclogites are exposed (Fig. 3). This variation in the Pan-African assemblages along the Ufipa Terrane may point to a southward directed subduction zone, above which high heat flow may have caused the high-temperature metamorphism in the upper plate (Fig. 12). The special distribution of mineral assemblages in the Ufipa Terrane, may as well communicate the presence of Pan-African paired metamorphic belts: In the north high P/T mineral assemblages (garnet–kyanite–white mica) are associated with eclogites and in the south the metapelites display low P/T mineral assemblages (garnet–cordierite).

The Pan-African suture between the Tanzania Craton and the Bangweulu Block is coeval with eclogite formation at ca. 530–500 Ma in northern Malawi (Fig. 12A; Ring et al., 2002) and the crustal thickening at ca. 530 Ma in the Zambezi Belt (Fig. 12B; John et al., 2003), which followed the subduction of oceanic crust between 659 ± 14 Ma and 607 ± 14 Ma (John et al., 2003, 2004).

The presence of Pan-African eclogites in the Ubendian Belt in combination with reworking of the country rocks in the Ufipa terrane and the intensive and extensive reworking of the Ubende Terrane to the north of the Ufipa Terrane (Boniface et al., 2012) suggest the existence of a Neoproterozoic suture zone in the Ubendian Belt, which resulted from the collision between the Tanzania Craton and the Bangweulu Block during the amalgamation of the Gondwana Supercontinent.

During the Proterozoic Eon the Ubendian Belt experienced repeated orogenic cycles, which were associated with subduction of oceanic lithospheres between 1890 and 1860 Ma (Boniface et al., 2012) and between 590 and 520 Ma (this study).

Acknowledgements

We thank DAAD and DFG (Sche 265/10) for funding this research. Our manuscript benefitted invaluably from the inputs of J.P. Liégois and K. Mezger during review. We value the contribution of A.H. Mruma during our second field campaign in 2006. We wish to thank T. John and the ICP-MS laboratory team of D. Garbe-Schönberg and his co-workers P. Fiedler and U. Westernströer for helping during sample preparation and analyses. We appreciate the assistance provided by P. Appel and B. Mader with microprobe analyses and A. Fehler for producing high quality thin sections. We

thank A. Larionov, I. Paderin, S. Presniakov and N. Rodionov a team of the SHRIMP laboratory at St. Petersburg and last but not least thanks to Nambunga for driving us during the first field trip.

References

Armstrong, J.T., 1995. Citzaf: a package of correction programs for the quantitative electron microbeam X-ray analysis of thick polished materials, thin films and particles. Microbeam Analysis 4, 117–200.

Black, L.P., Kamo, S.L., Allen, C.M., Aleinikoff, J.N., Davis, D.W., Korsch, R.J., Foudoulis, C., 2003. TEMORA 1: a new zircon standard for Phanerozoic U–Pb geochronology. Chemical Geology 200, 155–170.

Boger, S.D., Miller, J.M., 2004. Terminal suturing of Gondwana and the onset of the Ross–Delamerian Orogeny: the cause and effect of an Early Cambrian reconfiguration of plate motions. Earth and Planetary Science Letters 219, 35–48.

Boniface, N., Schenk, V., 2007. Polymetamorphism in the Paleoproterozoic Ubendian Belt, Tanzania. Geochimica et Cosmochimica Acta 71 (15 Suppl. S), A107.

Boniface, N., Schenk, V., Appel, P., 2012. Paleoproterozoic eclogites of MORB-type chemistry and three Proterozoic orogenic cycles in the Ubendian belt (Tanzania): evidence from monazite and zircon geochronology, and geochemistry. Precambrian Research 192–195, 16–33.

Boven, A., Theunissen, K., Sklyarov, E., Klerkx, J., Melnikov, A., Mruma, A., Punzalan, L., 1999. Timing of exhumation of a high-pressure mafic granulite Terrane of the Paleoproterozoic Ubende Belt (west Tanzania). Precambrian Research 93, 119–137.

Boynton, W.V., 1984. Cosmochemistry of the rare earth elements: meteorite studies. In: Rare Earth Element Geochemistry. Elsevier Sci. Publ, pp. 63–114.

Brock, P.W.G., 1963. The Mbozi Syenite–gabbro Complex. Unpublished Ph.D. thesis, University of Leeds.

Burchfiel, B.C., Deng, Q., Molnar, P., Royden, L., Wang, Y., Zhang, P., Zhang, W., 1989. Intracrustal detachment within zones of continental deformation. Geology (Boulder) 17 (8), 748–752.

Burchfiel, B.C., Royden, L.H., 1985. North-south extension within the convergent Himalayan region. Geology (Boulder) 13 (10), 679–682.

Clift, P.D., 1995. Volcaniclastic sedimentation and volcanism during the rifting of western pacific backarc basins. In: Active Margins and Marginal Basins of the Western Pacific, vol. 88. American Geophysical Union, Washington, DC, United States, pp. 67–96.

Collins, A.S., Pisarevsky, S.A., 2005. Amalgamating eastern Gondwana: the evolution of the Circum-Indian Orogens. Earth-Science Reviews 71, 229–270.

Corfu, F., Hanchar, J.M., Hoskin, P.W.O., Kinny, P.D., 2003. Atlas of zircon textures. In: Hanchar, J.M., Hoskin, P.W.O. (Eds.), Zircon. Reviews in Mineralogy and Geochemistry, vol. 53. Mineralogical Society of America and Geochemical Society, pp. 469–500.

Daly, M.C., 1988. Crustal shear zones in Central Africa: a kinematic approach to Proterozoic tectonics. Episodes 11 (1), 5–11.

Daly, M.C., Klerkx, J., Nanyaro, J.T., 1985. Early Proterozoic terranes and strike-slip accretion in the Ubendian Belt of southwest Tanzania. Terra Cognita (Abstract) 5, 257.

De Waele, B., Liégois, J.P., Nemchin, A.A., Tembo, F., 2006. Isotopic and geochernical evidence of Proterozoic episodic crustal reworking within the Irumide Belt of south-central Africa, the southern metacratonic boundary of an Archaean Bangweulu Craton. Precambrian Research 148 (3–4), 225–256.

Ellis, D.J., Green, D.H., 1979. An experimental study of the effect of Ca upon garnet–clinopyroxene Fe–Mg exchange equilibria. Contributions to Mineralogy and Petrology 71 (1), 13–22.

Ferry, J.M., Watson, E.B., 2007. New thermodynamic models and revised calibrations for the Ti-in-zircon and Zr-in-rutile thermometers. Contributions to Mineralogy and Petrology 154 (4), 429–437.

Garbe-Schönberg, C.D., 1993. Simultaneous determination of thirty seven trace elements in twenty-eight international rock standards by ICP-MS. Geostandards Newsletter, 17.

Gerya, T.V., Stockhert, B., Perchuk, A.L., 2002. Exhumation of high-pressure metamorphic rocks in a subduction channel: a numerical simulation. Tectonics 21 (6).

Graham, C.M., Powell, R., 1984. A garnet-hornblende geothermometer: calibration, testing, and application to the Pelona Schist, southern California. Journal of Metamorphic Geology 2, 13–21.

Hanson, R.E., 2003. Proterozoic geochronology and tectonic evolution of southern Africa. In: Proterozoic East Gondwana: Supercontinent Assembly and Breakup, vol. 206. Geological Society of London, pp. 427–463, Special volume.

Hawkins, J.W., 1995. Evolution of the lau basin; insights from odp leg 135. In: Active Margins and Marginal Basins of the Western Pacific, vol. 88. American Geophysical Union, Washington, DC, United States, pp. 125–173.

Hofmann, A.W., 1988. Chemical differentiation of the Earth: the relationship between mantle, continental crust, and oceanic crust. In: Isotope Geochemistry: The Crafoord Symposium, vol. 90(3), Amsterdam, Netherlands. Elsevier, pp. 297–314.

Holland, T.J.B., 1980. The reaction albite = jadeite + quartz determined experimentally in the range 600–1200 °C. American Mineralogist 65, 129–134.

Holland, T.J.B., Powell, R., 1998. An internally consistent thermodynamic data set for phases of petrological interest. Journal of Metamorphic Geology 16 (3), 309–343.

Hsue, K.J., 1991. Exhumation of high-pressure metamorphic rocks. Geology (Boulder) 19 (2), 107–110.

Hynes, A., Arkani, H.J., Greiling, R., 1996. Subduction of continental margins and the uplift of high-pressure metamorphic rocks. Earth and Planetary Science Letters 140 (1–4), 13–25.

Indares, A., Rivers, T., 1995. Textures, metamorphic reactions and thermobarometry of eclogitized metagabbros: a Proterozoic example. In: Fourth International Eclogite Conference, vol. 7(1). Schweizerbart'sche Verlagsbuchhandlung (Nägele u. Obermiller), Stuttgart, Federal Republic of Germany, pp. 43–56.

John, T., Klemd, R., Gao, J., Garbe-Schoenberg, D., 2008. Trace element mobilization in slabs due to non steady fluid-rock interaction: constraints from an eclogite-facies transport vein in blueschist (Tianshang, China). Lithos 103 (1–2), 1–24.

John, T., Schenk, V., Haase, K., Scherer, E., Tembo, F., 2003. Evidence for a Neoproterozoic ocean in south-central Africa from mid-oceanic-ridge-type geochemical signatures and pressure–temperature estimates of Zambian eclogites. Geology 31 (3), 243–246.

John, T., Scherer, E.E., Haase, K., Schenk, V., 2004. Trace element fractionation during fluid-induced eclogitization in a subducting slab: trace element and Lu–Hf–Sm–Nd isotope systematics. Earth and Planetary Science Letters 227 (3–4), 441–456.

Jöns, N., Schenk, V., 2008. Relics of the Mozambique Ocean in the central East African Orogen: evidence from the Vohibory Block of southern Madagascar. Journal of Metamorphic Geology 26 (1), 17–28.

Kelemen, P. B., Hanghøj, K., Greene A.R., 2003. One view of the geochemistry of subduction-related magmatic arcs, with emphasis on primitive andesite and lower crust. In: Rudnick, R. (Ed.), The Crust, vol. 3. Treatise on Geochemistry (Holland, H.D. Turekian, K.K (Eds.)), Elsevier–Pergamon, Oxford, pp. 593–659.

Klemd, R., Bröcker, M., 1999. Fluid influence on mineral reactions in ultrahigh-pressure granulites: a case study in the Snieznik Mts. (west Sudetes, Poland). Contributions to Mineralogy and Petrology 136 (4), 358–373.

Kohn, M.J., Spear, F.S., 1990. Two new geobarometers for garnet amphibolites, with applications to southeastern Vermont. American Mineralogist 75 (1–2), 89–96.

Koziol, A.M., 1989. Recalibration of the garnet – plagioclase – Al_2SiO_5 – quartz (GASP) geobarometer and applications to natural parageneses. EOS Transactions 70, 493.

Kusky, T.M., Abdelsalam, M., Tucker, R.D., Stern, R.J., 2003. Evolution of the east African and related orogens, and the assembly of Gondwana. Precambrian Research 123 (2), 81–85.

Lenoir, J.L., Liégois, J.P., Theunissen, K., Klerkx, J., 1994. The Palaeoproterozoic Ubendian shear Belt in Tanzania: geochronology and structure. Journal of African Earth Sciences 19 (3), 169–184.

Ludwig, K., 2001. SQUID 1.02. A Users Manual. Berkeley Geochronology Center Special Publication 2, 19.

McConnell, R., 1950. Outline of the Geology of Ufipa and Ubende. Bulletin 19, Geological Survey of Tanganyika.

Möller, A., Appel, P., Mezger, K., Schenk, V., 1995. Evidence for a 2 Ga subduction zone: eclogites in the Usagaran Belt of Tanzania. Geology 23 (12), 1067–1070.

Morimoto, N., Fabries, J., Ferguson, A.K., Ginzburg, I.V., Ross, M., Seifert, F.A., Zussman, J., Aoki, K., Gottardi, G., 1988. Nomenclature of pyroxenes. American Mineralogist 73 (9–10), 1123–1133.

Neal, C.R., Tylor, L.A., 1989. A negative Ce anomaly in a peridotite xenolith: evidence for crustal recycling into the mantle or mantle metasomatism? Geochimica et Cosmochimica Acta 53, 1035–1040.

Nie, S., Yin, A., Rowley, D.B., Jin, Y., 1994. Exhumation of the Dabie Shan ultra-high-pressure rocks and accumulation of the Songpan-Ganzi flysch sequence, central China. Geology (Boulder) 22 (11), 999–1002.

Pearce, J.A., 1996. A user's guide to basalt discrimination diagrams. In: Trace Element Geochemistry of Volcanic Rocks: Applications for Massive Sulphide Exploration, vol. 12. Geological Association of Canada, St. John's, NF, Canada, pp. 79–113.

Pearce, J.A., Cann, J.R., 1973. Tectonic setting of basic volcanic rocks determined using trace element analyses. Earth and Planetary Science Letters 19 (2), 290–300.

Perfit, M.R., Gust, D.A., Bence, A.E., Arculus, R.J., Taylor, S.R., 1980. Chemical characteristics of island-arc basalts: implications for mantle sources. In: Chemical Characterization of Tectonic Provinces, vol. 30(3). Elsevier, Amsterdam, Netherlands, pp. 227–256.

Powell, R., 1985. Regression diagnostics and robust regression in geothermometer/geobarometer calibration: the garnet–clinopyroxene geothermometer revisited. Journal of Metamorphic Geology 3 (3), 231–243.

Ray, G.E., 1974. The structural and metamorphic geology of northern Malawi. Journal of the Geological Society of London 130, 427–440.

Ring, U., Kroener, A., Buchwaldt, R., Toulkeridis, T., Layer, P.W., 2002. Shear-zone patterns and eclogite-facies metamorphism in the Mozambique Belt of northern Malawi, east-central Africa: implications for the assembly of Gondwana. Precambrian Research 116 (1–2), 19–56.

Rubatto, D., 2002. Zircon trace element geochemistry: partitioning with garnet and the link between U–Pb ages and metamorphism. Chemical Geology 184 (1–2), 123–138.

Sanders, I.S., Daley, J.S., Davies, G.R., 1987. Late Proterozoic high-pressure granulite facies metamorphism in the north-east Ox Inlier, north-west Ireland. Journal of Metamorphic Geology 5 (1), 69–85.

Sklyarov, E.V., Theunissen, K., Melnikov, A.I., Klerkx, J., Gladkochub, D.P., Mruma, A., 1998. Paleoproterozoic eclogites and garnet pyroxenites of the Ubende Belt (Tanzania). Schweizerische Mineralogische Petrographische Mitteilungen 78, 257–271.

Smirnov, V., Pentelkov, V., Tolochko, V., Trifan, M., Zhukov, S., 1973. Geology and minerals of the central part of the western rift. Tech. rep., Mineral and Resource Division, Dodoma, Tanzania. Unpublished report of the geological mapping.

Spear, F.S., Cheney, J.T., 1989. A petrogenetic grid for pelitic schists in the system SiO_2–Al_2O_3–FeO–MgO–K_2O–H_2O. Contributions to Mineralogy and Petrology 101 (2), 149–164.

Spear, F.S., Wark, D.A., Cheney, J.T., Schumacher, J.C., Watson, E.B., 2006. Zr-in-rutile thermometry in blueschists from Sifnos, Greece. Contributions to Mineralogy and Petrology 152 (3), 375–385.

Sun, S., McDonough, W.F., 1989. Chemical and isotopic systematics of oceanic basalts: implications for mantle composition and processes. In: Saunders, A.D., Norry, M.J. (Eds.), Magmatism in the Ocean Basins, vol. 42. Geological Society, Special Publications, London, pp. 313–345.

Sutton, J., Watson, J., James, T., 1954. A Study of the Metamorphic Rocks of Karema and Kungwe Bay, Western Tanganyika. Bulletin 22, Geological Survey of Tanganyika.

Tatsumi, Y., Hamilton, D.L., Nesbitt, R.W., 1986. Chemical characteristics of fluid phase released from a subducted lithosphere and origin of arc magmas: evidence from high-pressure experiments and natural rocks. In: Sakuyama, M., Fukuyama, H. (Eds.), Memorial Volume, vol. 29(1–4). Elsevier, Amsterdam, Netherlands, pp. 293–309.

Theunissen, K., Klerkx, J., Melnikov, A., Mruma, A., 1996. Mechanisms of inheritance of rift faulting in the western branch of the east African rift, Tanzania. Tectonics 15 (4), 776–790.

Theunissen, K., Lenoir, J.L., Liégois, J.P., Delvaux, D., Mruma, A., 1992. Major Pan-African imprint in the Ubendian Belt of SW Tanzania: U–Pb zircon geochronology and structural context. Comptes-rendus de l'Académie des Sciences de Paris 314, 1355–1362.

Tomkins, H.S., Powell, R., Ellis, D.J., 2007. The pressure dependence of the zirconium-in-rutile thermometer. Journal of Metamorphic Geology 25, 703–713.

Watson, E.B., Wark, D.A., Thomas, J.B., 2006. Crystallization thermometers for zircon and rutile. Contributions to Mineralogy and Petrology 151 (4), 413–433.

Whitney, D.L., Evans, B.W., 2010. Abbreviations for names of rock-forming minerals. American Mineralogist 95, 185–187.

Williams, I., 1998. U–Th–Pb geochronology by ion microprobe. In: McKibben, M., Shanks III, W., Ridley, W. (Eds.), Application of Microanalytical Techniques to Understanding Mineralizing Processes. Reviews in Economic Geology, vol. 7, pp. 1–35.